

An affordable upper limb prosthesis using Cognitive Computing and Brain-Computer Interface

Final Thesis

Nguyen Phuong Duy - s3518550
Supervisor: Pham Chi Thanh

Table of Contents

Table of Figures.....	3
Table of Tables	4
List of abbreviations.....	5
1. Executive summary	6
2. Introduction	7
3. Problem statement and research question.....	7
4. Literature review.....	7
4.1. Anatomical analysis	7
4.2. Neuroscience and neural engineering.....	8
4.3. EEG and BCI technology	9
4.3.1. 10 – 20 System.....	9
4.3.2. Motor imagery	9
4.3.3. Biofeedback	9
4.3.4. Visual Evoked Potential	9
4.3.5. BCI inputs.....	9
4.3.6. Hybrid BCI design.....	9
4.3.7. BCI hardware	10
4.4. Cognitive Computing	10
4.4.1. Machine learning classifier	10
4.4.2. Machine learning clustering	10
4.4.3. Independent component analysis	10
4.4.4. Computer vision.....	10
4.5. Biomaterial	11
4.6. Development boards and 3D printing technology	11
4.7. Limitations of conventional EMG prosthesis.....	11
4.8. Mechanical design.....	12
5. Research methodology	12
6. Results of experimental studies	14
6.1. Mechanical arm	14
6.1.1. Mechanical and electrical design.....	14
6.1.2. Control design.....	22
6.2. Brain-computer interface	24
6.2.1. Headwear.....	24
6.2.2. BCI electronics	25
6.2.3. BCI firmware	27
6.2.4. BCI functions.....	29
6.3. Hybrid active vision system	31
6.4. EMG sensor and elbow control	34
6.5. Final distributed system	34
6.6. User application.....	35
7. Project management.....	36
7.1. Time management and Work Breakdown Structure.....	36
7.2. Cost management	36
7.3. Risk management	37
8. Conclusion	38
9. Reference	39
10. Appendix.....	41
10.1. EEG DAQ analog board schematic.....	41
10.2. EEG DAQ digital board schematic.....	42

Table of Figures

Figure 1: Brain lobes and motor homunculus [15]	8
Figure 2: 10 - 20 system of EEG [17, 18]	9
Figure 3: Single-actuator mechanical finger design	12
Figure 4: Distributed system visualization	13
Figure 5: Modular block diagram	13
Figure 6: Sub-modules and interconnection diagram	14
Figure 7: Mechanical arm V1 complete design	14
Figure 8: Finger module 3D design assembly	15
Figure 9: Finger module design summary	16
Figure 10: Finger module printed with encoder	16
Figure 11: Palm plate and thumb module design	16
Figure 12: Linear actuator 3D design and printed	17
Figure 13: Wrist joint with linear actuator, design and 3D printed	17
Figure 14: Wrist rotor gear design and 3D printed	17
Figure 15: Hand module and wrist module fit test	18
Figure 16: Hand dorsal design and complete hand module printed	18
Figure 17: Complete wrist design assembled	18
Figure 18: Fully assembled transradial prosthesis	18
Figure 19: Elbow and forearm design summary	19
Figure 20: Final transhumeral prosthesis 3D design	19
Figure 21: Mechanical arm electronic system	20
Figure 22: Complete transhumeral prosthesis, normal form (left) and rotated form (right)	20
Figure 23: Elbow gear box and springs	21
Figure 24: Design dimension comparison	21
Figure 25: Cylindrical grip (bottle), spherical grip (ball) and tripod grip (tape roll)	22
Figure 26: Point grip, lateral grip (key) and hook grip (paper roll)	22
Figure 27: Tip pinch grip (microchip) and random grip (screwdriver)	22
Figure 28: First version of watchdog timer with button and OLED interface	23
Figure 29: EEG headwear and electrode spring-loaded mechanism	24
Figure 30: DRL ear clip design and printed	25
Figure 31: Spike and no-spike reusable electrode for EEG	25
Figure 32: BCI modules interconnection	25
Figure 33: EEG analog circuit block diagram	25
Figure 34: Analog board, digital board and DAQ board	26
Figure 35: Active electrode schematic and implementation	26
Figure 36: BCI final headwear	27
Figure 37: Effect of delay pulses on FFT analysis	28
Figure 38: FFT function credibility test with 10-second, 5-second and 2-second window	28
Figure 39: Dual-channel BCI – software and hardware	29
Figure 40: Alpha trigger test recorded using designed BCI	29
Figure 41: SSVEP test result - 10 Hz (blue), 15 Hz (orange), 20 Hz (green) and 25 Hz (red)	30
Figure 42: SSVEP maze test - signal view with 20 Hz trigger (left) and 25 Hz trigger (right)	30
Figure 43: Training total loss after 4000 steps – TensorBoard view and detailed graph view	31
Figure 44: Evaluation image after 1500 steps	31
Figure 45: Evaluation image after 2500 steps	31
Figure 46: Evaluation image after 3500 steps	31
Figure 47: Model deployment on Raspberry Pi	31
Figure 48: Pan-tilt module with tracker test	33
Figure 49: Hybrid vision with cloud - test on mechanical arm - side view	33
Figure 50: Hybrid vision with cloud - test on mechanical arm – front view	34
Figure 51: EMG schematic and PCB 1-layer design	34
Figure 52: Alpha trigger targeting hand module	35
Figure 53: Hybrid active vision targeting object and picking object up	35

Figure 54: Sample hand patterns and end-user application for customization and debugging	36
Figure 55: Gantt chart for project management, starting November 2018 to December 2018.....	36
Figure 56: EEG analog board schematic.....	41
Figure 57: Impedance tester sample circuit.....	41
Figure 58: EEG digital board schematic.....	42

Table of Tables

Table 1: Mechanical arm phase 1 detailed module information	14
Table 2: New mechanical design modules and parts information.....	15
Table 3: Benchmark test result	21
Table 4: DOF improvement result.....	21
Table 5: Serial packet format and value	23
Table 6: Default hand figure packet in controller	24
Table 7: Different raspberry pi models CV performance comparison	31
Table 8: Different tracker comparison	32
Table 9: New CV model performance comparison	33
Table 10: New CV system with cloud server performance comparison	33
Table 11: EMG action mapper	34
Table 12: Cost analysis based on market research and purchase history	37
Table 13: Updated risk management.....	38

List of abbreviations

<i>Abbreviations</i>	<i>Definition</i>
<i>AI</i>	Artificial Intelligence
<i>API</i>	Application Programming Interface
<i>BCI</i>	Brain-Computer Interface
<i>BOM</i>	Bill of Material
<i>CC</i>	Cognitive Computing
<i>CMRR</i>	Common-Mode Rejection Ratio
<i>COCO</i>	Common Objects in Context
<i>CSI</i>	Camera Serial Interface
<i>CV</i>	Computer Vision
<i>DAQ</i>	Data Acquisition
<i>DFT</i>	Discrete Fourier Transform
<i>DOF</i>	Degree of Freedom
<i>DRL</i>	Driven Right Leg
<i>EEG</i>	Electroencephalography, brain signal
<i>EMG</i>	Electromyography, muscle signal
<i>ERP</i>	Event-Related Potential
<i>FPS</i>	Frame per Second
<i>GND</i>	Ground
<i>ICA</i>	Independent Component Analysis
<i>KTL</i>	Kanade-Lucas-Tomasi
<i>LED</i>	Light-Emitting Diode
<i>mAP</i>	Mean Average Precision
<i>MEG</i>	Magnetoencephalography
<i>MI</i>	Motor Imagery
<i>ML</i>	Machine Learning
<i>O</i>	Occipital lobe
<i>OLED</i>	Organic Light-Emitting Diode
<i>P</i>	Parietal lobe
<i>PCB</i>	Printed Circuit Board
<i>PID</i>	Proportional – Integral – Derivative
<i>PLA</i>	Polylactic Acid
<i>RX</i>	Receive
<i>SoC</i>	System on Chip
<i>SSD</i>	Single Shot Multibox Detector
<i>SSVEP</i>	Steady State Visually Evoked Potential
<i>TX</i>	Transmit
<i>VDD</i>	Power supply
<i>VOC</i>	Visual Object Classes
<i>WBS</i>	Work Breakdown Structure

1. Executive summary

The study of prosthesis market shows an opportunity to develop a low cost, functional and intuitive solution. The literature review proposed the use of brain-computer interface (BCI), machine learning and active computer vision to create a hybrid prosthesis controlled by brain rhythm, muscle signal and camera. It is stated that the final product must be low cost, functional, durable, scalable, intuitive and user friendly.

The design methodology includes the modularization of large system into sub-systems and modules to further be engineered based on the corresponding field of research. The entire project is broken down to two sub-systems of the electroencephalography (EEG) sub-system and the mechanical arm sub-system. The headwear, or EEG sub-system, is responsible for acquiring brain rhythm, following by action classification. The arm controls the mechanical movement and the muscle trigger consciously executed by user. Throughout the described process, the computer vision finds the object of interest and chooses the corresponding hand figure, tracks the object and manipulates the object when received an executive trigger from the user.

Through several design iterations, the final mechanical arm is divided into 4 modules of hand modules, wrist module, forearm module and elbow module. The hand module consists of 4 finger modules, each of which has 1 Degree of Freedom (DOF), and a thumb module of 2 DOF. The wrist consists of two linear actuators and a third pivot point to bring about 2 DOF of tilting and waving. The rotator is added between the wrist and the forearm, proving the design with 1 more DOF. The forearm holds all electronics and power supply for the entire system and is positioned beneath the spring-loaded elbow module. The final design has 10 DOF and able to perform complex movements and wide range of dexterity: cylindrical, spherical, tripod, tip pinch, lateral, hook, point and platform. The BCI consists of three modules of analog board, digital board and Data Acquisition (DAQ) board. The analog board has a gain of 8000, with cut-off frequency of 59 Hz. The DAQ board samples EEG signals into a 1500 single-bit data points serial packets and sends them to BCI main controller. The current BCI could perform alpha trigger and Steady State Visually Evoked Potential (SSVEP), with 10, 15, 20, 25 Hz stimuli. The final SSVEP could perform with high detection ratio while only running 5-second window. The hybrid vision system consists of a 20-object object recognition, an object tracker and a cloud server to bring about an autonomous solution for the prosthesis in real time. The system works well with all chosen hardware and is benchmarked on Raspberry Pi Zero W to have an average performance of 5 frames per second (FPS) offline and 10 FPS online. The final distributed system is put together, with SSVEP used to choose the module of interest, alpha trigger used to execute commands on the chosen module while hybrid active vision used to control wrist module autonomously. Electromyography (EMG) is used to control elbow module or executes emergency interrupt when a module is malfunctioned.

Overall, the project is timely managed, the objectives are met, and the cost analysis shows feasibility and scalability of the proposed system. The final transhumeral prosthesis is a 10 DOF mechanical arm that could perform complex movements and maintain high level of dexterity while being limited with control inputs. This design is to support amputee and congenital limb deficiency patients, whose muscles are abnormal and incapable of generating required inputs for EMG. The project takes post-assembly upgrade and maintenance into consideration to bring about a complete support system, with numerous control schemes offered by the design, cloud server for performance and model update, and user application to personalize hand grip patterns.

The project has several limitations. One of which is the use of non-invasive electrode that hinders better EEG and EMG signal acquisition. The BCI currently only supports SSVEP and alpha trigger, which also needs further research to implement motor imagery and left-right coordination.

Future work includes coming back to Vietnam for system field trial with a congenital limb deficiency patient that has previously been tested with EMG and shown positive results, working on motor imagery for BCI and designing a smaller headwear for mobility and ease of installation.

2. Introduction

Amputation is a surgical process that involves removing a limb from a human due to either medical illness, trauma or surgery. According to the International Diabetes Federation, number of diabetes patients is increasing every year. It is also reported that for every 30 seconds, a lower limb or a part of a limb is amputated due to diabetes [1]. Among the leading traumatic causes of limb amputation are war (27.1%), other unintentional injuries (18.4%), falls (13.3%), mechanical forces (10.5%) and road injuries (8.1%). Accounting for those numbers, there are 273,949 cases in South Asia and 114,268 cases in East Asia within 1.2 million people having major limb amputation because of traumatic causes globally in 2015 [2]. The post-traumatic stress affects heavily the mental health. There is also study that find the correlation between anxiety and depression development and amputation [3]. This implies the necessity of prosthesis to help amputees regain mobility and independence in life throughout rehabilitation.

However, prosthesis market in United States study shows a revenue of 1.85 billion USD in 2013. For upper limb prosthesis, the cost could vary from 5,000 USD without any function to 30,000 USD or more for a cosmetically realistic myoelectric hands and a neuro-prosthetic arm could cost as much as 100,000 USD [4]. This makes prosthesis unaffordable for most amputees despite the rising need.

Technology is pacing fast with the rise of Brain-Computer Interface (BCI) [5] and 3D printing. This makes prosthesis gradually be more accessible and affordable. Despite the development, prosthesis still lacks function to support complex movement sequence, further improvements after installation or mobility. Therefore, an improved approach to create a low-cost prosthesis with post-installation development and adaptability could be a solution to current constraints.

This project aims to develop a hybrid system combining Cognitive Computing (CC) with BCI following modular design to provide amputees with an affordable solution that could overcome current limitations and further improve independence and mobility for wielding individuals. The result is a hybrid distributed system running BCI and electromyography (EMG) for executive control, and active computer vision for automatic action planning in real time. The final design enables congenital limb deficiency patients and amputees to control a 10-degree-of-freedom prosthesis with limited inputs.

3. Problem statement and research question

Following the market research [1-5], the demand for prosthesis is on the rise yet the current solutions on the market is too expensive for consumers and amputees with average income. On the other hand, despite the advancement of technologies, current prosthesis still lacks mobility and functionality. It is thus suggested that the proposed solution of this project must satisfy the following objectives:

- The prosthesis must be able to carry out a range of different tasks, supporting amputee in daily and social life. The prosthesis must not be a burden to the user but rather be a tool.
- The attachment and detachment process of prosthesis could be carried out by amputee alone. The size and weight of prosthesis is also designed for usage convenience.
- Prosthesis is scalable and upgradable for long-term usage.
- Prosthesis is fail-safe, has long runtime and has user-friendly design.
- Prosthesis must be affordable in comparison with current solutions on the market [4].
- Prosthesis is easy to control and collaborative with the user, high in interaction and intuitive.

4. Literature review

A comprehensive literature review helps determine the most appropriate and feasible design concept for the problem statements, showing the gap in technologies and knowledge, the current methods and the possibilities.

4.1. Anatomical analysis

The project targets at upper limb, above elbow prosthesis and thus there are more demands in design than which of lower limb prosthesis. The human arm has 7 degrees of freedom (DOF) excluding the hand, and the human hand alone consists of more than 20 DOF [6, 7], this indicates a sophisticated mechanical design solution for the hand and the robotic arm and also requires a complex control method to bring about a seamless experience while maintaining dexterity.

For transhumeral prosthesis, long transhumeral [8] shall be addressed, and prosthesis will be attached to the upper arm. Subsequently, biceps brachii muscles and triceps brachii muscles [9] are the muscle groups that will be in direct contact with the prosthesis for attachment, detachment or any further control methods.

The mean segment weights of human body part analysis [10] shows that the total arm accounts for an average of 5% of the total body weight across both genders and upper arm is 3%. Moreover, it is determined that the average weight in Asia is 57.7 kg, and average

body mass globally is 62 kg [11], with 45 kg for children [12]. Thus, the weight constraint and design metric of the final system will be 2.25 kg to be usable for all age groups and nations.

4.2. Neuroscience and neural engineering

The human brain consists of neurons, which are considered the basic computational unit of the nervous system [13]. A neuron receives hundreds of inputs from others, processes information and forwards to other hundreds. When a neuron receives a strong input from others, on the cell membrane, the neurotransmitters activate the ion channels thus let neurons exchange ions with the extracellular space. This potential change generates electric fields which can then be measured [13]. Although the potential field created by a neuron is insufficiently strong to be read, the propagation of that signal to hundreds and thousands closely situated neurons result in a potential sum that could be measured. It can be summarized from this process that electroencephalography (EEG) reflects the excitation and inhibitory of postsynaptic potentials summation [14]. The below figures show the brain regions and the motor homunculus:

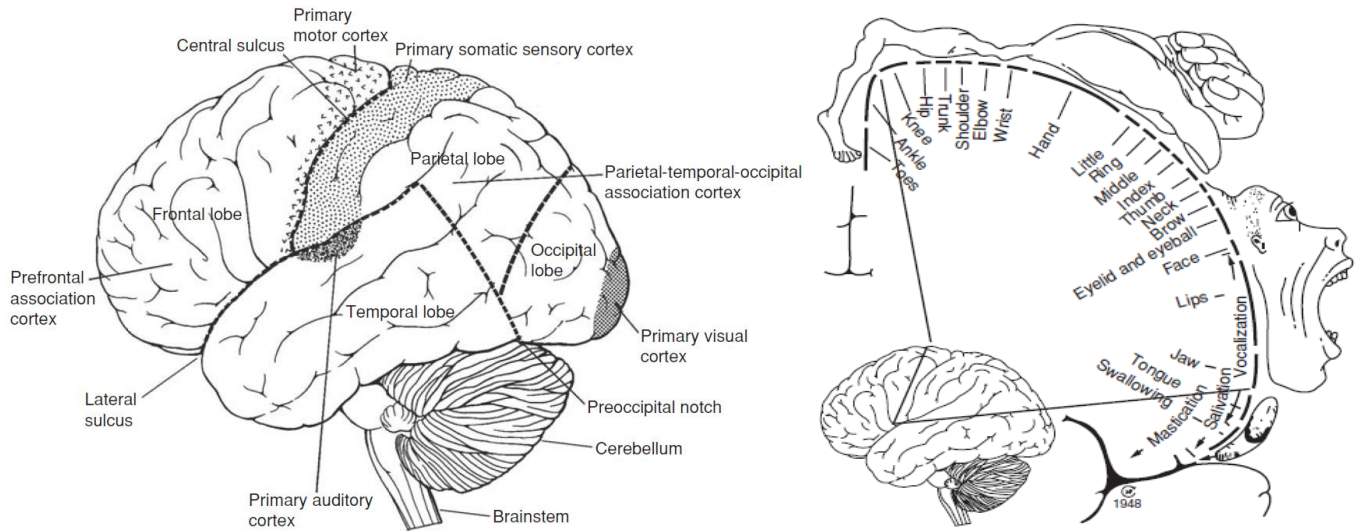


Figure 1: Brain lobes and motor homunculus [15]

The figures show the scalp location to measure brain signal. As the project targets rehabilitation for amputee in motor action, the motor cortex is examined. By allowing a small current through parts of the brain, neurosurgeons and scientists have found distinct functions allocated with different region of the human brain. Through electrical stimulation, the motor homunculus is identified.

It is also derived from the figure that different regions of the primary motor cortex are depicted to hold a specific control corresponding to a body part. Along the intersection of the frontal lobe and the parietal lobe is the primary motor cortex (along the central sulcus). From this, it is reported that the primary motor cortex is not the only brain region contributing to the motor control, but the adjacent somatosensory cortex also involves. In fact, though stimulating the primary motor cortex shows connection to the body parts, it is identified that there are more than 50 areas [15] involved in the control motor action. An action could be divided into four dimensions for research and understanding of time (planning or execution), encoding (abstract or concrete coding of action), complexity (simple or complex movement) and source (internal-driven desire or external-driven desire) regarding the motor control hierarchy. Hence, the motor homunculus only shows the effect of electrical stimulation on human, and even though the neuronal activity of primary motor cortex is closely related to that of movement muscles, the action itself and corresponding signal processing of the brain is too complex to be directly used and control the prostheses.

Brain rhythms are separated into bands of delta (2 – 4 Hz), theta (4 – 8 Hz), alpha (8 – 12 Hz), beta (15 – 30 Hz), lower gamma (30 – 80 Hz) and upper gamma (80 – 150 Hz). There are faster rhythms of up to 600 Hz, yet most cognitive processes could be represented using only frequencies from 2 – 150 Hz [14]. On the other hand, people suffering from amputation and congenital limb deficiency usually have brain signal rewired at the damaged nerves, called neural reorganization [16]. Thus, their neural activation patterns are aberrant [15] and could not be based on other normal individuals.

4.3. EEG and BCI technology

4.3.1. 10 – 20 System

The following figure shows the 10 – 20 system in BCI system:

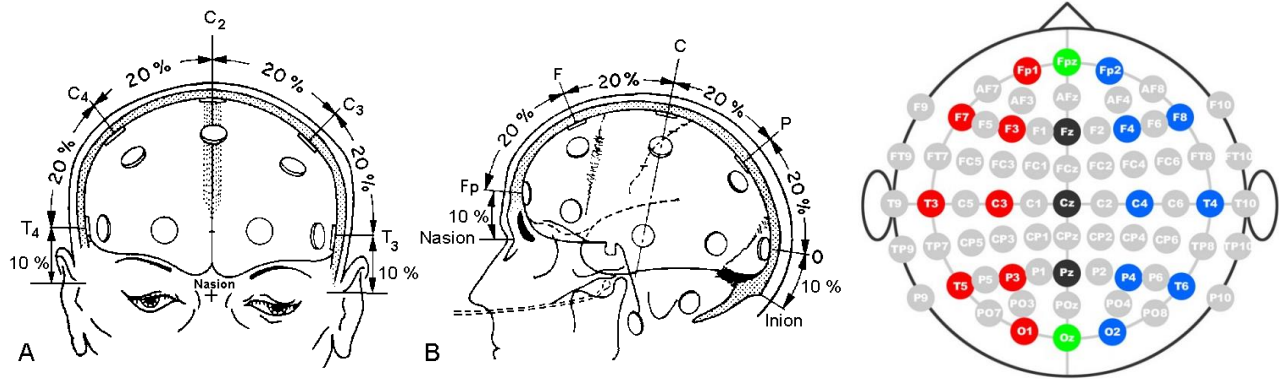


Figure 2: 10 - 20 system of EEG [17, 18]

The 10 – 20 system shows the optimal location for positioning electrodes. The scalp dimension is firstly measured, and the electrodes are then positioned either 10% or 20% of that, depending on the required resolution. Following the position of the probes are the corresponding name of the location based on the respective lobe, with Prefrontal (Fp), Occipital (O), Parietal (P), Frontal (F), Temporal (T) and Central (C).

4.3.2. Motor imagery

From research of the hierarchy in planning and executing of a motor action, if a user imagines an action of a body part and the brain signal and the potential action are concurrently measured, the sensorimotor cortex will present oscillations that could be measured and analyzed. Hence, by imagining the wanted action, the planning process of the brain will give out signal, which can then be decoded and used to control a brain-computer interface application [16].

4.3.3. Biofeedback

Biofeedback is the process of achieving awareness of the physiological functions using instruments applied on the same system to reflect the activities, with the objective to finally learn to control those functions at will [16]. Biofeedback takes in account four brain rhythms of theta, alpha, beta and sensorimotor rhythm (SMR) from 12 to 15 Hz. It is thus suggested that biofeedback could provide BCI with more control channels. Biofeedback could be a solution to neural reorganization in amputee and congenital limb deficiency patients, through which they could eventually learn to generate corresponding signals to drive the system.

4.3.4. Visual Evoked Potential

Visual Evoked Potential, or VEP, is the electrical potential recorded when there is a visual stimulation applied on the subject. SSVEP, or Steady-State VEP is one of the most common VEPs [16]. In SSVEP-based BCI, the subject is presented with different patterns flashing on screen, with each pattern mapped to an action or a command. By measuring the brain section that is responsible for visual action while the subject focuses on a pattern on screen that matches the action, the EEG will show correlation with frequency spectrum of the pattern. This could then be decoded into the mapped action and used to drive an external device. SSVEP-based BCI allows user to choose the wanted action by means of looking at blinking patterns or a repetitive visual trigger.

4.3.5. BCI inputs

There are two most common approach for measuring potential action of human brain: EEG and magnetoencephalography (MEG). Among them, EEG is easy to assemble, easy to setup and cheaper whereas MEG does not need gel to function and works well with brain signals of high frequency. This is due to magnetic field can be transmitted through scalp without any loss [14]. For EEG, it is also studied that, maintaining a minimal number of electrodes of 8 would result in an accuracy of 90% [19] for BCI systems.

4.3.6. Hybrid BCI design

There have been bodies of work across institutes and research groups around the world conducting researches on BCI and EEG for the past decades [16]. Among the existing BCIs, the most common ones are P300 event-related potentials, sensorimotor rhythms, steady-state visual evoked potentials (SSVEP), electrocorticography activity, motor cortex, premotor cortex and brain metabolic signals [16]. Of those interfaces, SSVEP and motor imagery (MI) are the most implemented due to robustness and low-cost configuration [20-23].

There have been numerous researches conducted using a hybrid system combining motor imagery and SSVEP to acquire a more accurate and precise result in classifying brain signals. Most of which focus on C3, C4 and Cz [20-23] of the 10-20 system [18] as BCI inputs and thus this set of electrodes will be used for this project.

Considering the SSVEP design, a study found that wide-band SSVEP with frequencies of 10, 15, 20, 25 Hz achieves 90% of detection ratio [24]. It is thus suggested that the final SSVEP system will include visual triggers of those frequencies.

4.3.7. BCI hardware

There are several references to design low-cost and functional BCI system using EEG through open-source projects and research platforms. Some of many are OpenBCI [25] and OpenEEG [26]. There are also research papers and university projects such as [27, 28] that refer to a low-cost and sufficient implementation of BCI.

4.4. Cognitive Computing

4.4.1. Machine learning classifier

As discussed in the neuroscience of neuro engineering, the brain signals corresponding to an action, from planning to executing, are complicated and consist of several brain regions in cooperative for decision making. This suggests the need to use a machine learning classifier as an artificial neural network to predict the wanted action through several signal inputs from multiple electrodes. The prediction model can be trained by asking the user to think of an action from a set of predefined actions to be executed and brain signals are simultaneously recorded to build the classifier for the final BCI.

Of the current BCI technologies, both motor imagery and VEP are built and implemented with machine learning algorithms for classification and prediction [29, 30].

4.4.2. Machine learning clustering

Another approach of using machine learning in the study and research of brain signal and EEG is the use of unsupervised methods for brain signal feature extraction, finding the unknown correlations between the recorded signal and the demanded actions [31]. Machine learning clustering methods could be used to group signals with high correlation and thus the patterns could be obtained. An example of unsupervised learning is k-means clustering, with an attempt to group n observations to k clusters in which the observation is grouped to the cluster with the nearest mean.

4.4.3. Independent component analysis

Independent component analysis, or ICA, is usually used in signal processing to separate signal sources from each other. As following the 10 – 20 system and the motor homunculus, the electrodes could pick up adjacent signals and thus lack of accuracy and resolution. By using ICA, distinct signals could be obtained for further analysis with higher accuracy and better resolution. There are researches on using ICA to separate Event-Related Potentials (ERPs) of brain signal such as in [32].

4.4.4. Computer vision

Computer vision, though hardly seen in prosthesis, is growing rapidly in its separated domain of vision in cognitive computing. Due to the recent advancement in machine learning algorithms and convolutional neural network, computer vision could execute object detection, object classification fast enough for real-time application and embedded system. Thus, within a system, computer vision could be developed as a stand-alone sub-system to singularly or help others solve a practical engineering problem such as in [33].

The system implements a hybrid active vision system running object recognition and object tracking. The object recognition database are referenced from the following projects of Microsoft COCO (Common Objects in Context) [34] and PASCAL Visual Object Classes (VOC) [35]. The project uses TensorFlow to train and evaluate the object recognition model for the system based on TensorFlow Object Detection API and the training models and algorithms performance metric refers to the respective research [36].

Robustness of object tracking system is the ability to detect faulty detection and tracking and reject, restart the tracking process. There have been studies on the matter, following by different solution and tracking progress alternatives [37, 38]. On the other hand, object tracking in real-time implementation has been proven to be resource-consuming and with low accuracy [38, 39]. Specifically in active vision system, the saccade movement hinders the tracking process [40], as well as further problems with overshooting and undershooting of control system. It is thus important for an active tracking system to be robust, be responsive, work well with lack of resource and have high accuracy.

The development of advanced algorithms and models for machine learning based object recognition leads to the proposal of applying them to the tracking process. By implementing object recognition, the object of interest could be chosen and tracked autonomously. This brings about robustness and mobility to the system. It is thus important to consider different algorithms available and choose the

most suitable one for real time application. A research on speed and accuracy of different convolutional models for object recognition [36] suggests the use of MobileNet SSD for its highest mean average precision (mAP) among the algorithms designed for real-time application.

Kalman filter, optical flow and KLT algorithm are among the most mentioned methods for object tracking [39, 41]. Despite the strengths in either accuracy or simplicity in implementation, object trackers lack robustness and ability to scale with the object, specifically when the object gets closer or further away. Among the tracking algorithms, Median Flow could address both robustness and depth concurrently. Median Flow is based on Forward-Backward error and has been proven to achieve better performance than most traditional trackers [42]. Assuming there is a sequence of image S as followed:

$$S = (I_t, I_{t+1}, I_{t+2}, \dots, I_{t+k})$$

Let x_t be the point of interest at time t . If a tracker is applied to track x through k steps, the resulting trajectory could be expressed as followed, with f denotes forward tracking process:

$$T_f^k = (x_t, x_{t+1}, x_{t+2}, \dots, x_{t+k})$$

After getting the tracking trajectory, point x_{t+k} is tracked backward using sequence S to result in another trajectory as followed, with b denotes backward tracking process:

$$T_b^k = (\hat{x}_t, \hat{x}_{t+1}, \hat{x}_{t+2}, \dots, \hat{x}_{t+k})$$

The different between the two trajectories are computed and is defined as the Forward-Backward error [42], with the difference is calculated using Euclidean distance:

$$FB(T_f^k | S) = distance(T_f^k, T_b^k) = \|x_t - \hat{x}_t\|$$

By apply this to multiple points within the bounding box, with 50% of the worst predictions omitted, an object is successfully tracked. On the other hand, the scale change could also be computed by getting the median of all ratios of distance between each current point at its previous corresponding point. For Median Flow, the tracker used to compute the point trajectory is Lucas-Kanade tracker [42].

4.5. Biomaterial

Considering the biomaterial used for the project, the electrodes play an important role in both acquiring EEG and EMG and connecting the human and machine. It is then compulsory for the electrodes to be of biomaterial type for long-term usage and be harmless to the amputee when in continuous skin exposure. There are two types of commercial electrodes, being dry electrode with Ag/AgCl base and wet electrode with gel, both need to be medical grade.

Regarding the electrode installation, there are invasive and non-invasive. The invasive electrode will be implanted and thus gives better result and resolution whereas the non-invasive one will be positioned outside and thus give poorer accuracy and performance.

4.6. Development boards and 3D printing technology

Recent advancement in technology leads to high demand in low-cost, high-computational and small development boards with diverse external and internal peripherals for general usages. The rise of system-on-chip (SoC) provides a means of thorough and efficient solution in developing and prototyping, with high support in real time application and embedded system and cross-platform compatibility.

3D printing is gradually re-defining small scale manufacturing and prototyping, supporting more materials, with wider range of strength-to-weight ratio and higher resolution. Depending on usage and requirements, 3D printing could be used to construct complex interior structure and mechanical parts for machinery and robotics.

It is also studied that polylactic acid, or PLA in 3D printing, is proven safe and usable for medical application [43] and thus the use of 3D printing will greatly reduce the weight and cost of prosthesis while maintaining the medical-grade property and highly customizable.

4.7. Limitations of conventional EMG prosthesis

Market research and literature review of upper limb prostheses show a wide range of current options and the overall limitations towards the functions and mechanical design. Among the solutions, most of which are transradial type [44], and most electric prostheses are designed for below elbow amputation. In general, there are three types of commercial prosthesis of electric,

myoelectric and body-powered [44]. Considering myoelectric, a challenge is that the number of input channels is significantly less than the output ones. There are also numerous limitations regarding the extraction of EMG signals: the EMG signal of everyone is different and thus the controller needs to be tuned individually; the change in arm position will result in subsequent change in EMG signal; the placement of electrodes will also result in EMG signal change and fatigue of the used muscle for EMG signal acquisition will also reduce the read result [45]. There are previous studies emphasizing that a multifunctional myoelectric prosthetic hand will require at least 4 months of daily training [45].

There are different experiments conducted with different number of EMG sensors, ranging from 2 to 32, resulting in a conclusion that the system performs better with more sensors, but not extremely, whereas the increment in prosthesis cost due to excessive use of EMG sensors suggests lessening the sensor number [45]. The use of myoelectric sensors is too expensive on average and will also make the device more fragile compared to other alternatives [44].

Considering the functions of current prostheses, to mimic more natural movements, some are equipped with 2 or more microprocessors [46]. The number of grip types available is highly important, as it plays a crucial role in determining how useful the prosthesis is in practical use [45]. However, as the number of grips increases, the system will take time to browse through the options and could eventually become cumbersome and slow [45]. To tackle this problem, some prostheses rely on the user manually selecting the thumb position (opposed or non-opposed) with an additional toggle button to switch between grip groups. Thus, they have two DOF in control of close command and open command [45]. It is also worth mentioning that among the current prostheses, humeral rotation is an advantage as it has not been reported. In addition, it is also the movement that every amputee loses [46].

From a survey conducted regarding the prioritization of features to be enhanced for myoelectric prosthesis, the most crucial improvements needed are the ability to move the fingers and thumb separately, the ability to prevent the objects from slipping, the adaptation of grip strength, the increment of the wrist range of motion, the weight of the final prosthesis and noise reduction [47]. As discussed in [48], a basic set of 8 canonical hand postures could be used as an early performance metric for the mechanical design: cylindrical, lateral, point, tripod, tip, hook, platform and spherical. The modular designs of prosthesis hand and finger are also assessed and analyzed, which study in [49] gives reference and guidance to the design and evaluation.

4.8. Mechanical design

The project aims at modularity and thus cannot follow one of the common prosthesis designs to put motors in forearm and use wires to control fingers. One of the reasons is the following limitation of the wrist movement and the wrist modularization process. It is then suggested that all the mechanical movements of the hand module should be positioned within the hand itself. There are numerous studies and design concepts following this approach, one of which is the following research which refers to several single-actuator mechanical finger designs [49]:

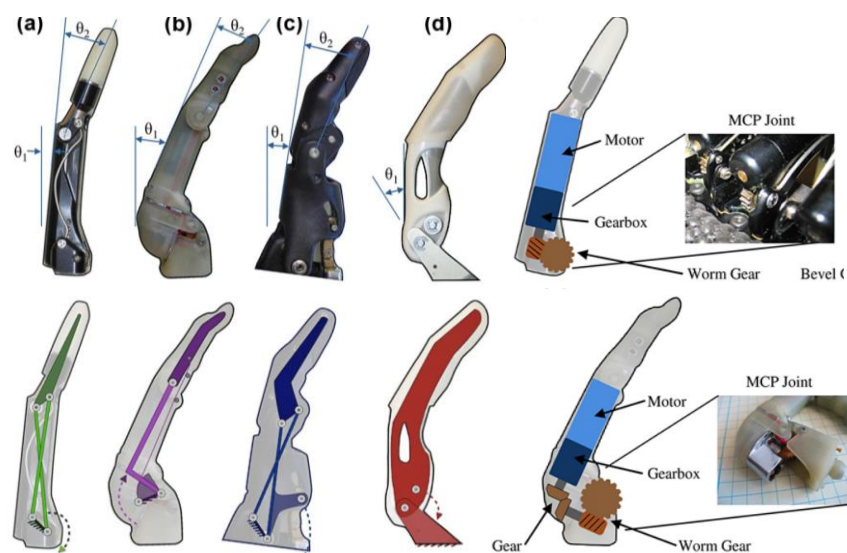


Figure 3: Single-actuator mechanical finger design

5. Research methodology

The entire system is modularized and distributed, physically and functionally, to have better overall control, customization and scalability. There are three main controllers within the system supporting each other for the best cost performance: EMG, EEG and CV. Their cooperation is designed as followed:

- EEG will be responsible for the monitoring of brain rhythm using SSVEP and motor imagery to determine the actions being thought of by the user.
- The mechanical arm will then receive commands from EEG module and wait for EMG to be triggered before starting the execution of the action sequence. The EMG is also used to control the elbow movement based on the level read from muscle activity at the attachment point.
- When that sequence of action is being execute, CV will look for the respective object in front of the prosthesis to choose the corresponding hand figure based on object size and shape using object classification. CV will also be used to control the wrist to face the palm at the object of interest using object tracking algorithm.

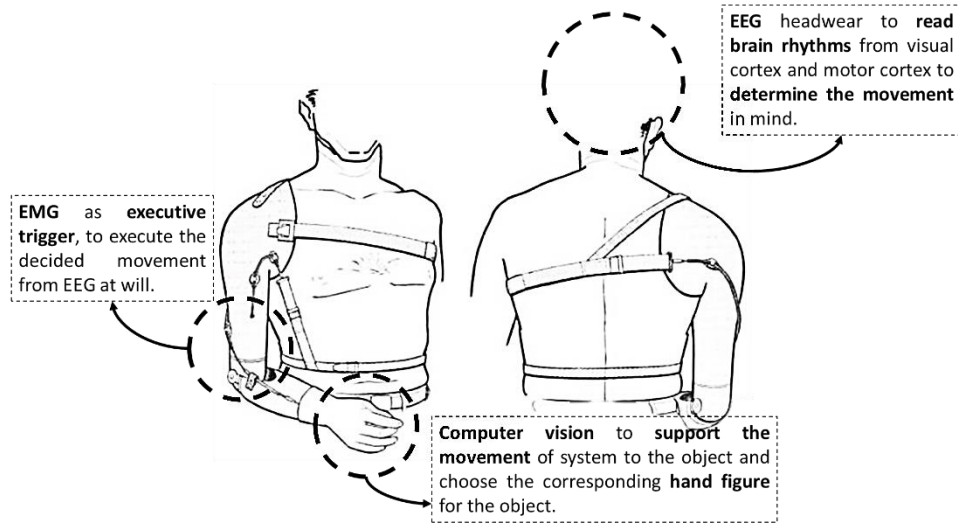


Figure 4: Distributed system visualization

The combination of all three controllers will help the system do complex movement, be fail-safe and intuitive to control. The following figure depicts the building blocks of the system in detail:

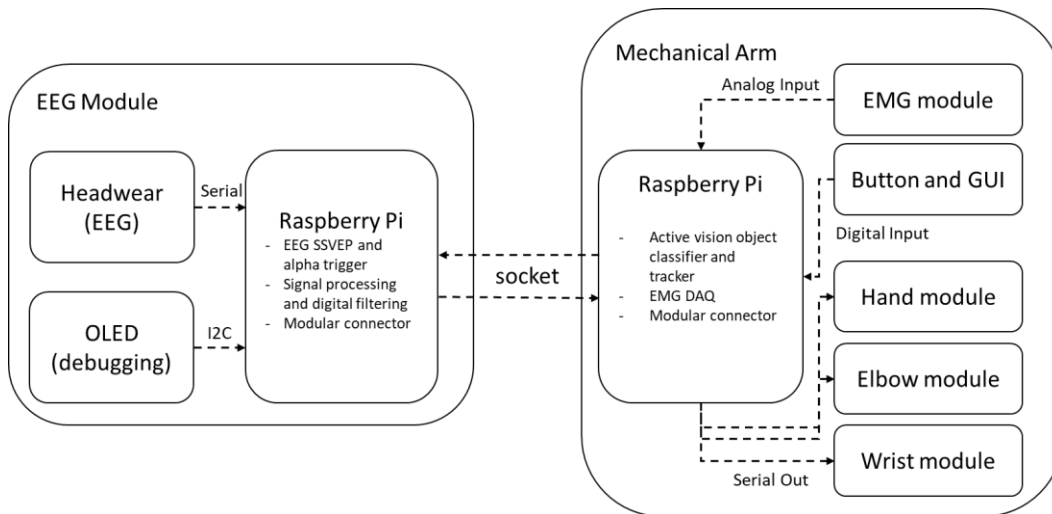


Figure 5: Modular block diagram

As the design of EEG data acquisition module requires medical grade components and materials, with proportionally high cost, the use of CV can help release the computational stress on BCI and lower the overall system developing and manufacturing expense. As for using 3D printing, the prosthesis is customizable, lightweight and low-cost. For the scalability nature of the project, the system is broken down to subsequent modules. This makes the system both self-organized and collaborative, upgradable and easy to maintain. The latest system design iteration adds in a dedicated cloud server to speed up heavy computational processes. This allows the system to perform complex tasks in real time. The following figure shows the interconnections of the entire system:

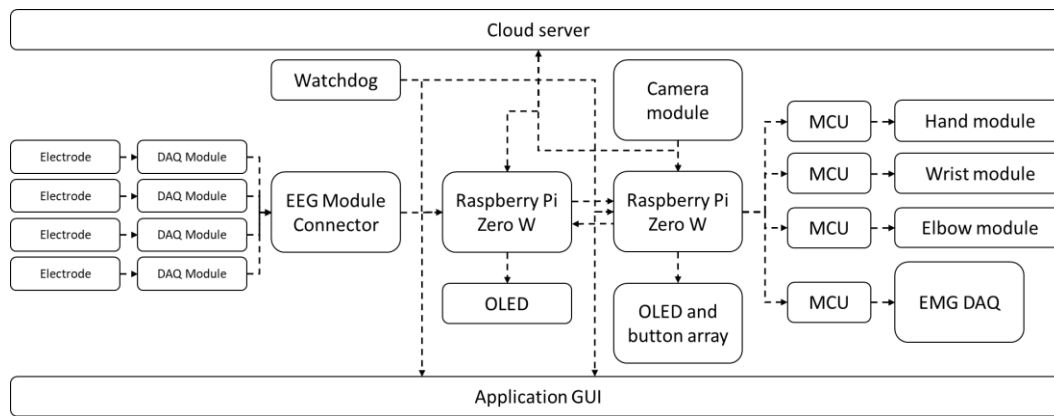


Figure 6: Sub-modules and interconnection diagram

6. Results of experimental studies

The following section summarizes all the findings throughout the research to thoroughly reflect the improvements.

6.1. Mechanical arm

6.1.1. Mechanical and electrical design

The mechanical arm version 1 (V1) design is divided into 4 modules: hand, wrist, forearm and elbow. The following figure shows design V1 of mechanical arm:

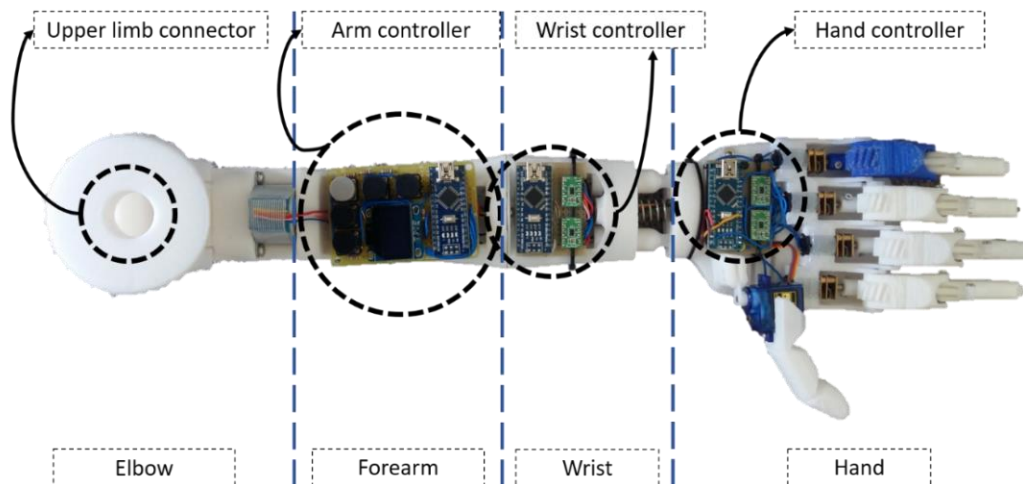


Figure 7: Mechanical arm V1 complete design

The following table shows the detailed information of each module:

Module	Usage	Inputs	Outputs	DOF
Hand module	Support grip patterns and object manipulation.	Serial packet from controller	Individual finger calibration and complete hand grip pattern.	5
Wrist module	Control palm position of hand module.		Difference in linear actuator length cause angular offset to the pivot of the hand module.	1
Forearm module	Housing for battery and electronics.	n/a	n/a	0
Elbow module	Connection point of prosthesis, support vertical movement for the prosthesis.	Serial packet from controller	A worm gear box drives the angle of the elbow.	1
Watchdog module	Control the timing of all modules, pass serial packets to modules from main controller, emergency calibration, debugging session.	Buttons	OLED and serial packets to other modules.	0
Total				7

Table 1: Mechanical arm phase 1 detailed module information

The V1 design has a total of 7 DOF. This design, although usable, has numerous weaknesses:

- There has not been any support for control feedback. The controller of each module remembers the number of pulses and the apparent position of the joints based on that number of pulses. This control method requires the user to adjust all the joints to home position before and after usage to maintain the accuracy. If there is not enough power supply and/or a joint is offset due to external impact, the controller will not be informed, and the joint will be driven wrongly.
- The hand module is a single unit consisting of 4 fingers and a thumb. This has been proven to be a weak design through practical implementation and developing process of phase one. As if a finger is broken, the entire hand module needs to be replaced and re-assembled.
- The thumb, designed to only have 1 DOF, is insufficient for complex hand grip patterns as suggested in [48].
- The wrist design has proven to be too weak to handle the object weight. The current wrist design also does not solve the humeral rotation as discussed in literature review and does not have feedback mechanism to support controller.
- The elbow design is not strong enough to withstand the overall moment force applied by object weight at the hand module.

From the weaknesses of design V1, alternatives are considered, and the entire mechanical arm is redesigned. The final design, or design version 2 (V2) is also divided into 4 subsequent mechanical modules of hand, wrist, forearm and elbow. However, each subsequent module is further broken down into smaller parts, with different functions though sharing a single controller. The following table shows the subsequent modules, parts and controllers of the new mechanical design:

Sub-module	Sub-part	Function
Hand module	Finger	Base part of index, middle, ring and pinky
	Thumb	Thumb of the hand module
	Palm	Hold the fingers and thumb together
	Hand dorsal	Hold the electronics and connect to wrist
Wrist module	Linear actuator	Provide movement for wrist
	Ball joint system	Define movement limit and trajectory
	Ball bearing system	Support wrist rotation and wrist extension
	Wrist gear set	Provide movement for humeral rotation
Forearm module	n/a	Battery pack, electronics housing and prosthesis extension
Elbow module	Elbow gear box	Provide up/down movement for prosthesis
	Humeral connector	Connect to humerus end
	Forearm connector	Connect to forearm module
Watchdog module	Local controller	Provide debugging, synchronization, emergency control
	Network controller	Connection endpoint of distributed system

Table 2: New mechanical design modules and parts information

The design V2 has 10 DOF, with 6 for hand module, 3 for wrist and 1 for elbow. The design V2 is to overcome the limitations and lack of robustness of V1, giving the user partial humeral rotation (located at the wrist), full range of wrist motion and a hand module capable of providing all suggested 8 canonical grip patterns [48]. Each joint of design V2 is equipped with encoder to further improve control and interaction and no longer require user to manually calibrate home positions of each joint before and after usage.

The design V2 is grouped into two main sub-designs. The first sub-design consists of the hand module and wrist module, which could be used as a stand-alone transradial prosthesis. The second sub-design consists of the forearm module and elbow module. The combination of both sub-designs brings about the final transhumeral prosthesis. The detailed design of the parts of the hand module is shown below:

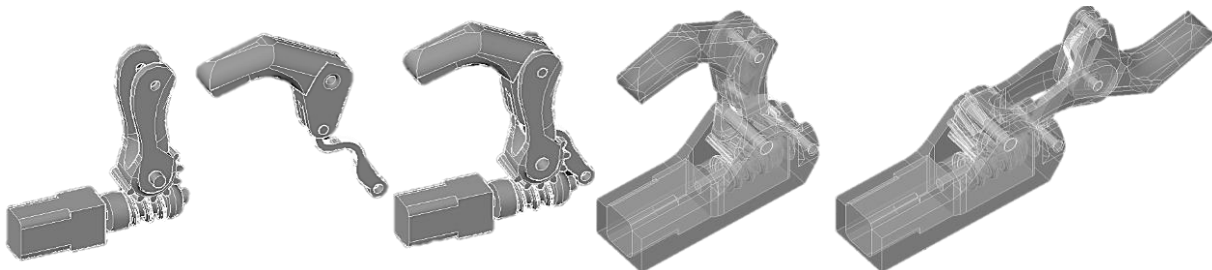


Figure 8: Finger module 3D design assembly

3D assembled

2D assembled

Exploded 3D view
with color-coded parts

Trajectory design
based on color-coded parts

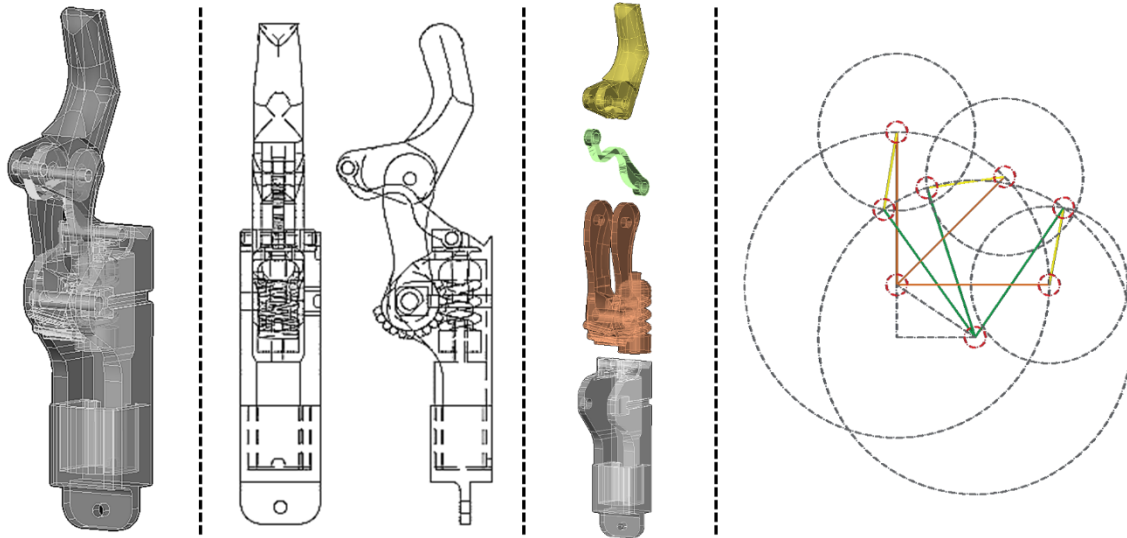


Figure 9: Finger module design summary

The figure shows the trajectory of the finger curl and the realization in 3D modelling. The new finger is also equipped with encoder at the side of the body to support control feedback. The encoder used is a potentiometer and is installed into the shaft.



Figure 10: Finger module printed with encoder

The design of pinky, ring, middle and index fingers are similar and could be reused. The thumb design consists of a servo motor for 1 DOF and half of the finger design for the other 1 DOF, also equipped with encoder at the side. The palm is a plate with 4 slots for 4 finger modules and a connector for thumb module. The palm plate and the thumb design are shown in the following figures:

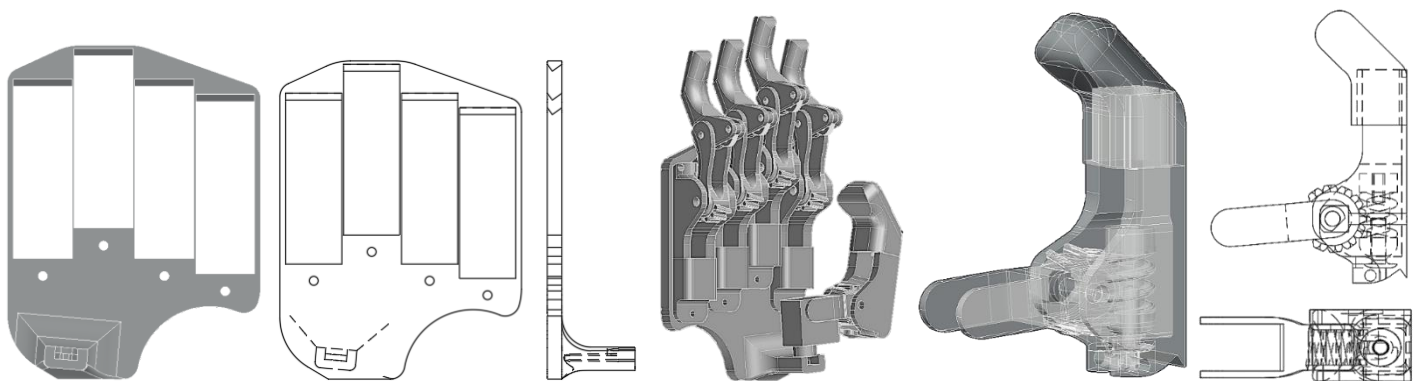


Figure 11: Palm plate and thumb module design

The new wrist module of V2 consists of 4 smaller parts: linear actuator, top connector, bottom connector and rotator. The linear actuator is redesigned to have a slide potentiometer to feedback the current position. The 3D design and assembly are shown below:

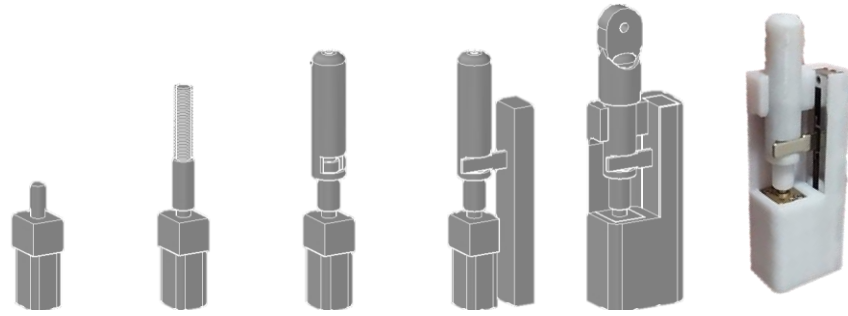


Figure 12: Linear actuator 3D design and printed

The linear actuator has a range of 2 centimeters, with full span duration of 10 seconds. A pair of linear actuators positioned apart from each other, with another pivot on the same plane forming an isosceles triangle, could provide the wrist with two ranges of motion: upward – downward and left – right curl, corresponding to tilting motion and moving motion. When the motor rotates, the threaded rod inside the linear actuator gradually moves either into or out of the linear actuator, causing the overall distance between the contact point of the hand module and the wrist module to change accordingly. The designed linear actuator could extend up to 2 centimeters and as for the actuators are positioned 3 centimeters away from each other, the effective offset angle is approximately $\arctan(2/3) = 35$ degree. To allow the wrist to freely move, the third pivot is a ball joint and is designed as followed:

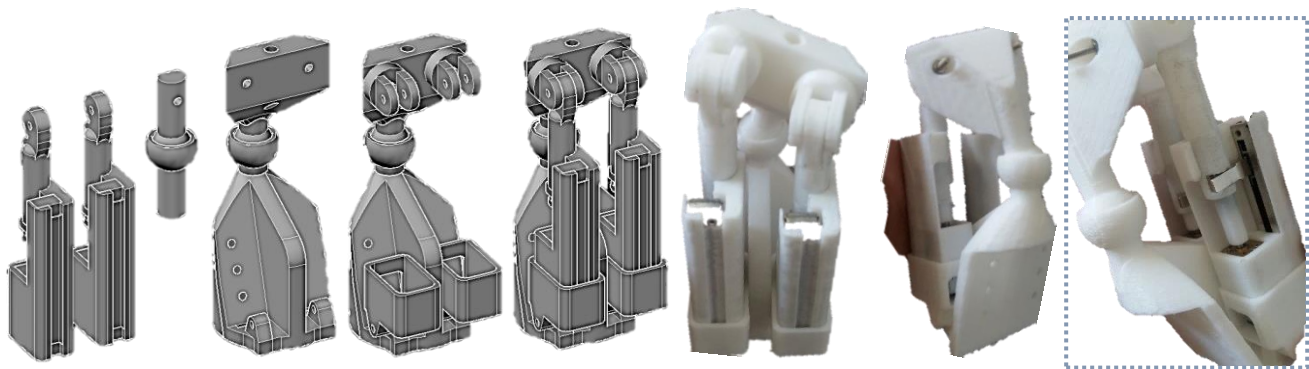


Figure 13: Wrist joint with linear actuator, design and 3D printed

As seen from the above figure, the bottom connector holds two linear actuators and connected with the top connector through the ball joint. The rotator is a gear set designed to further support the wrist will partial humeral rotation and wrist rotation. To decrease friction and utilize 3D printing technology, a ball bearing is designed within the rotator. The rotator is connected to the bottom connector. The rotator 3D design and assembly are shown below:

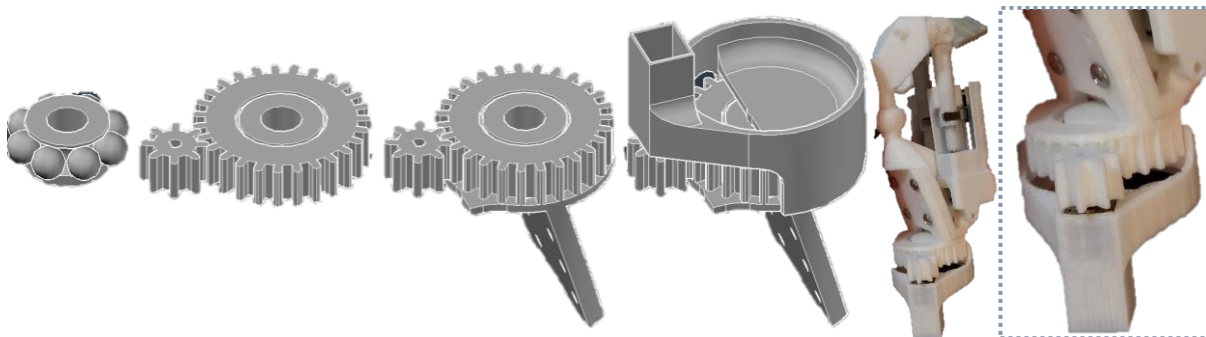


Figure 14: Wrist rotor gear design and 3D printed

When the wrist and the hand module have been designed, the hand dorsal is lastly designed. The hand dorsal both serves as the electronics housing for the hand module, and the connector between the hand module and the wrist module. Thus, the hand dorsal is lastly designed. The hand module and the wrist module are placed closed together for dimension and fit test:

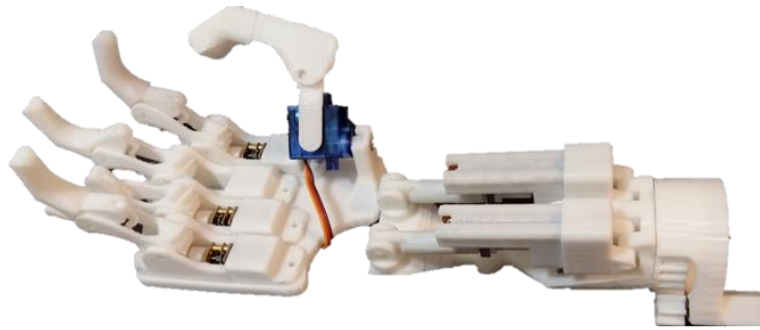


Figure 15: Hand module and wrist module fit test

The hand dorsal is then design and the implementation is shown below. The design V2 of hand module overcome all listed limitations of V1, further improving the system dexterity and scalability.

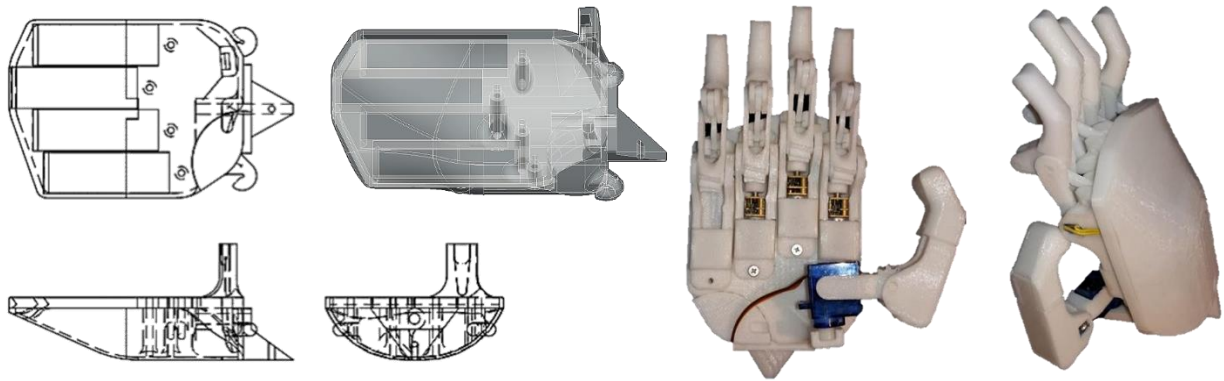


Figure 16: Hand dorsal design and complete hand module printed

There are also two pairs of hooks added to the hand dorsal and wrist module, which will later be used to support a set of springs. The springs will act as tendons connecting the wrist module and the hand module. The final wrist module is assembled and shown. A shield is added to the back of the wrist to protect the electronics:

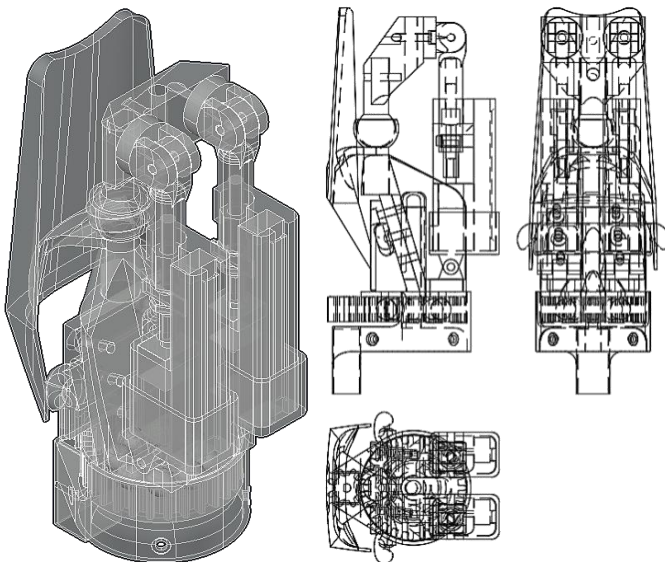


Figure 17: Complete wrist design assembled

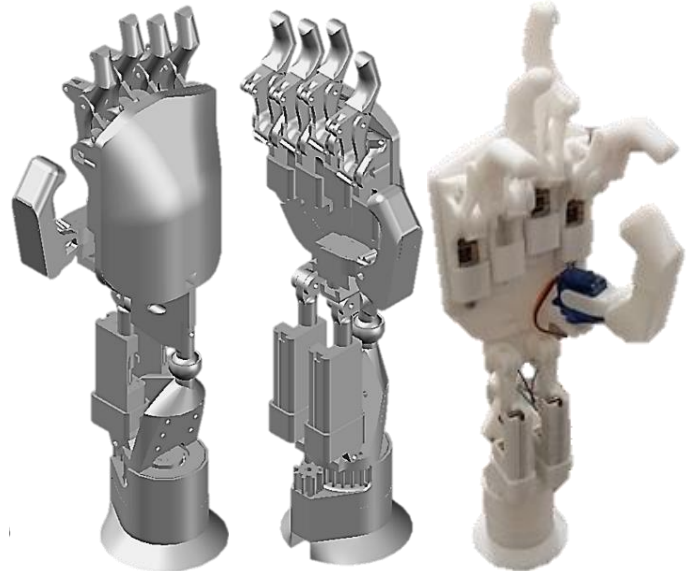


Figure 18: Fully assembled transradial prosthesis

The new wrist design of V2 has 3 DOF and overcomes all limitations of V1. The triangular configuration of the three pivots evenly distributes the force applied and supports the wrist in handing objects being manipulated by the hand module. A complete look of the final assembly of the new hand module and new wrist module is shown in the above figure. This sub-system alone could be used as a transradial prosthesis for below-elbow amputation.

The forearm and elbow are merged and redesigned. The elbow is also designed to be spring-loaded. The forearm holds the power supply of the entire system. Thus, the forearm is positioned under the elbow to minimize the moment of force applied on the elbow rotor. The design summary of the elbow and forearm is shown below:

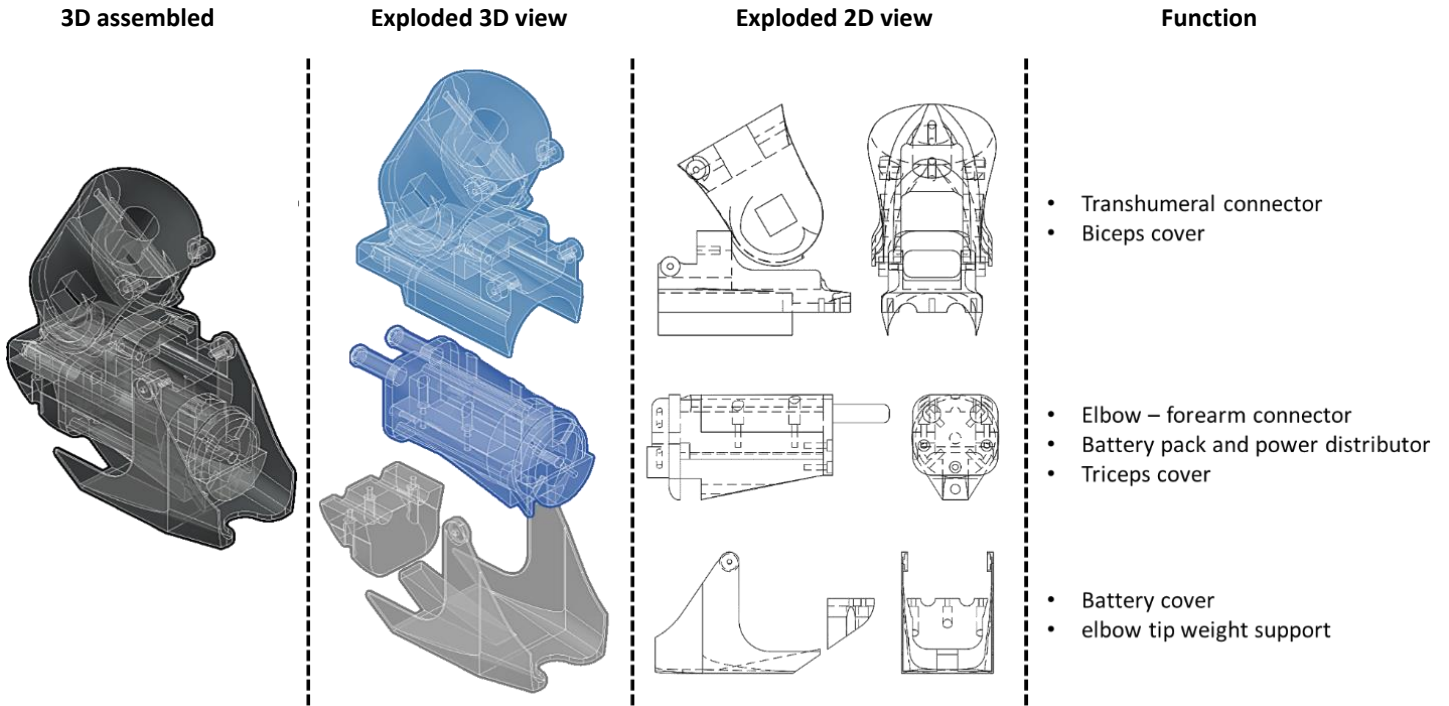


Figure 19: Elbow and forearm design summary

The two sub-designs are combined to create the final transhumeral prosthesis. The final 3D design of V2 is shown below:

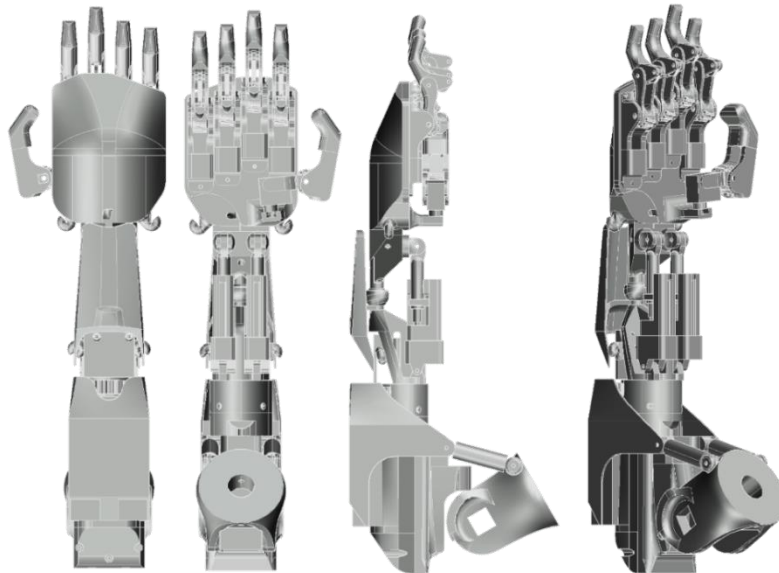


Figure 20: Final transhumeral prosthesis 3D design

Before further working with the elbow, all the electronics are assembled onto the prosthesis. This is to get the most correct measurement of the weight applied on the elbow, which will later be calibrated accordingly to support prosthesis. The electronics includes power supply, voltage regulators for motors and microcontrollers, all controllers of all modules, main controller and wiring. The electronics of the entire mechanical system is simplified and shown in the following figure:

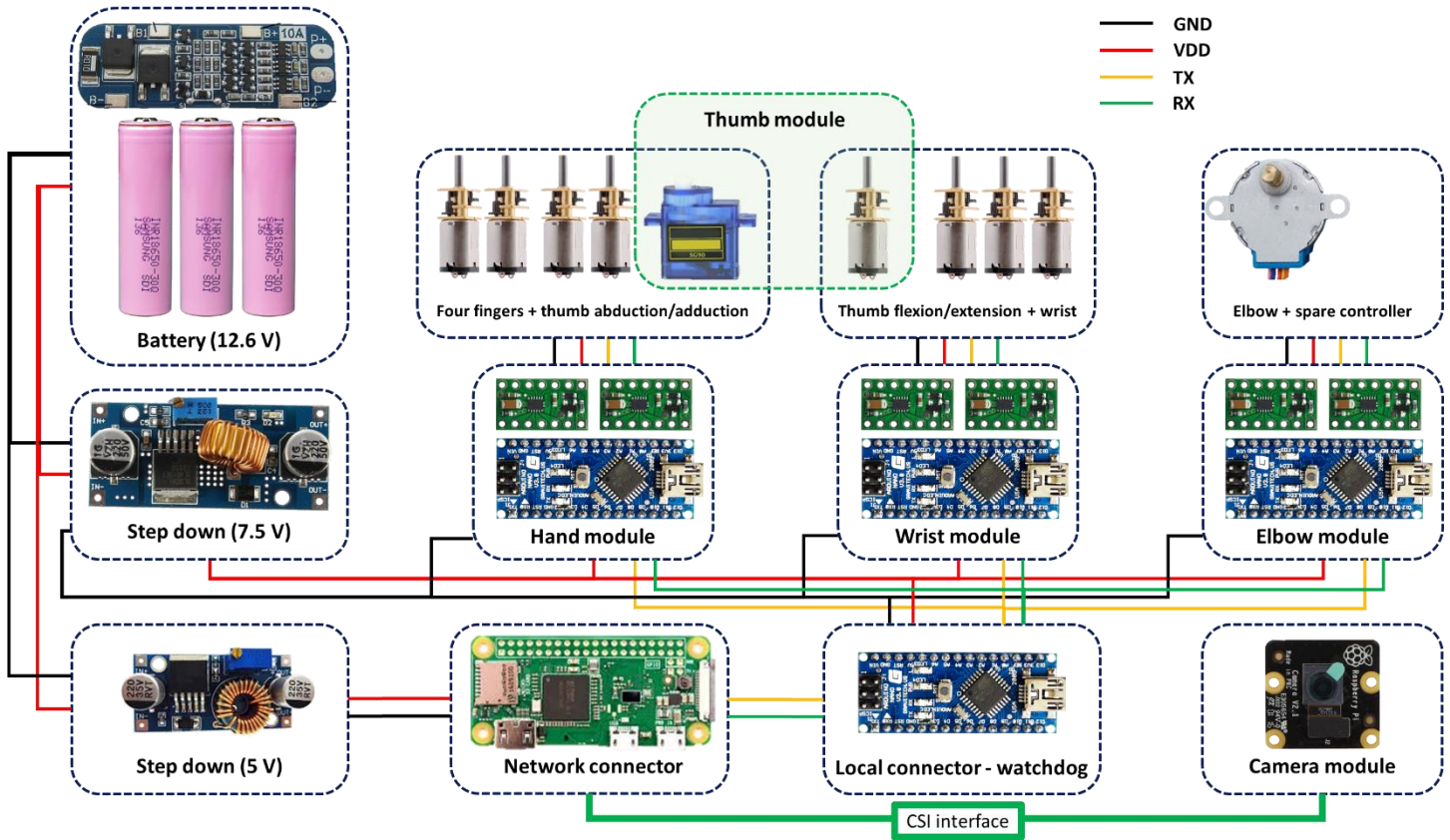


Figure 21: Mechanical arm electronic system

It is derived from the schematic that each mechanical module is controlled by a separate controller, with a local controller maintaining system stability and forwarding serial packets from network connector to all parts of the mechanical arm. Each controller is determined with an ID, which will then be compared with the ID encrypted in the serial packet to only execute commands stored in corresponding packets. The control system for the mechanical arm could be found in [Control design](#). The electronics are wired and the final transhumeral prosthesis is shown in the following figures:

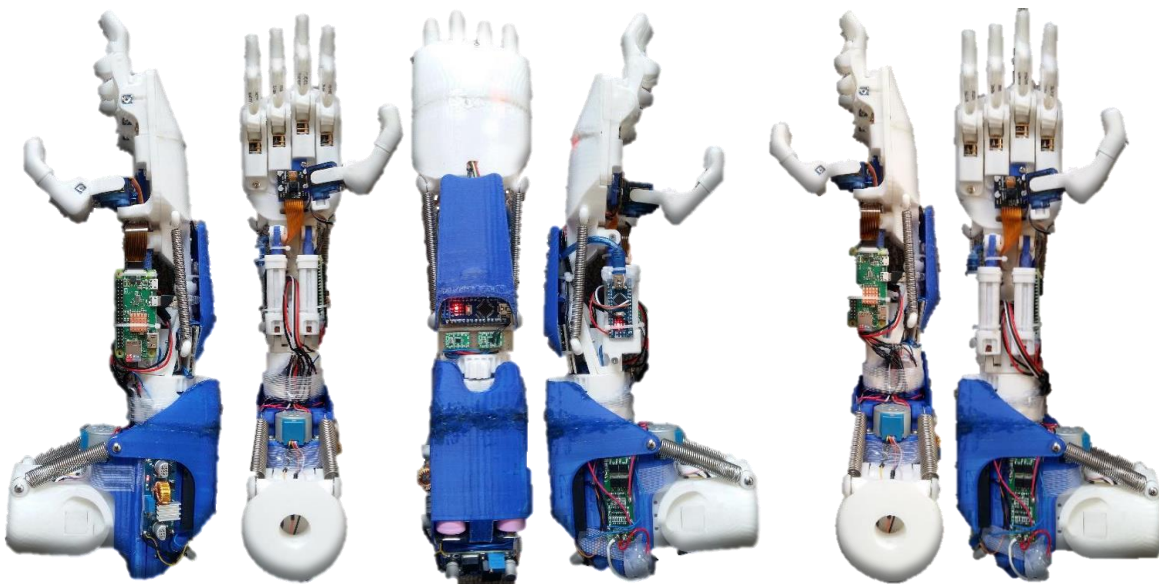


Figure 22: Complete transhumeral prosthesis, normal form (left) and rotated form (right)

Lastly, the elbow is calibrated to support the weight of the complete prosthesis. The elbow consists of a 29:1 gear box with two springs attached outside. By changing the springs, the optimized balance could be found, and the elbow could eventually lift the prosthesis. The following figures show the parts mentioned:



Figure 23: Elbow gear box and springs

The prosthesis is then benchmarked. The following table shows the result of all the tests run:

Specification		Design V1/metric	Design V2
Weight		Less than 2.25 kg	970 g
Wrist	Left – right curl	60°	60°
	Up – down curl	n/a	30°
	Rotate	n/a	180°
Finger curl		90°	90°
Thumb	Flexion/extension	n/a	180°
	Abduction/adduction	180°	180°
Elbow	Curl	90°	90°
	Weight capacity	n/a	800 g (90°) – 100 g (30°)
Battery	Continuous use	n/a	6 hours
	Idled	n/a	12 hours
	Full charge	n/a	3 hours

Table 3: Benchmark test result

Module	Design V1	Design V2
Hand module	5	6
Wrist module	1	3
Forearm module	0	0
Elbow module	1	1
Total	7	10

Table 4: DOF improvement result

The tables show prospective results, and visible improvements acquired in the design V2 of the mechanical arm. The overall dimension of the design is compared, and the result could be seen below:

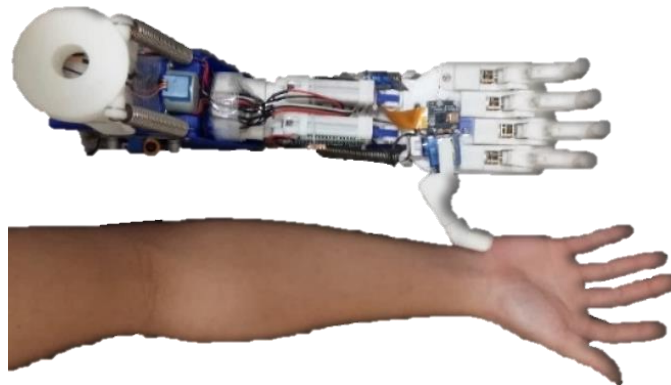


Figure 24: Design dimension comparison

The design is smaller than the dimension of an adult arm, and thus could be scaled to be usable for both adults and children. Following the research on a robust design of prosthesis with a defined test case of 8 canonical hand patterns [48], the following figures show the corresponding dexterity of the design:



Figure 25: Cylindrical grip (bottle), spherical grip (ball) and tripod grip (tape roll)



Figure 26: Point grip, lateral grip (key) and hook grip (paper roll)



Figure 27: Tip pinch grip (microchip) and random grip (screwdriver)

Of all the grip patterns shown, the tip pinch grip is one of the most important and is also the most neglected one in numerous commercial prosthesis. The current design could successfully carry out this grip pattern for all four fingers.

6.1.2. Control design

Controlling the hand module is a separate controller consists of 4 H-bridge motor drivers and a microcontroller. External peripherals could communicate or control the hand module by connecting to 4 pre-defined wires of 5V, GND, transmit (TX) and receive (RX). The local controller, or the separate hand controller, is responsible for the external communication and internal control process, meaning the controller only receive a single command or control packet from external communication and the following series of action is self-organized for execution. As the design methodology aims at modularization, the control interface must be straightforward for the main controller and all the heavy and complex computations are done at local level.

Practical measure of motor performance with respect to torque-speed curve of the chosen motor when being supplied with 7.5V 1A shows a 90-degree motion duration of 3600 milliseconds. Thus, the default resolution is 1 degree per step, corresponding to a duration of $3600/90 = 40$ milliseconds. This control resolution is only applied for index, middle, ring, pinky fingers and flexion/extension of thumb. Abduction/adduction movement of thumb is driven with servo motor, which could be easily controlled. By controlling the motors using step duration to switch the H-bridge and remembering the current step or the cumulative steps of a motor, the next

motor action can be planned accordingly. The recent design iteration adds in encoder to all fingers, which can be used to check for current position and calibrate if necessary.

The controller of wrist module has 4 H-bridge motor drivers and a microcontroller. As the wrist only has 3 motors to control, and the hand module lacks 1 driver for the new thumb movement, 1 H-bridge from wrist module is eventually used to support hand module. There are also 4 pre-defined wires of 5V, GND, TX and RX for the control interface of the wrist module.

The elbow module has its dedicated controller. The stepper motor is controlled in a bipolar fashion, with 4 phases, speed variation ratio of 1/64 and in-traction torque higher than 34.3 millinewton meter at 120 Hz.

There is a watchdog timer and main controller designed and positioned on the complete arm to maintain system stability and accuracy throughout runtime. The first design takes the following form:



Figure 28: First version of watchdog timer with button and OLED interface

The initial idea behind the button and OLED display is to provide user with an interface to calibrate individual modules to home position, test all available functions for debugging purpose or to interrupt and reset any modules when error arises. However, the latest design omitted the interface and kept only the microcontroller to save space. This interface, however, is still usable and could connect to the mechanical design instantly through the defined 4-pin socket (5V, GND, TX, RX) to gain executive control when needed.

Currently, this controller supports bilingual interface of Vietnamese and English. The controller has 7 basic modes of individual finger calibration, command hand figure, control wrist movement, control elbow movement, calibrate SSVEP stimuli, check battery status and watchdog timer.

The watchdog timer is a function of this controller, to which the controller will frequently request I2C packet from any module configured as I2C slave. The respective module will send back a packet depicting the current working condition and thus from this process, if any module fails to reply to the I2C master command of the controller, it will be interrupted and reset to prevent any harmful errors from happening.

For serial connection, the standard packet format is as followed:

Mode	Data 0	Data 1	Data 2	Data 3	Data 4
2 Bytes	1 Byte				

Using a similar packet structure across all modules within the sub-system, the difference is shown in the following table:

Module	Mode	Data 0	Data 1	Data 2	Data 3	Data 4	Description
Hand	0	Thumb data: 0 – 180	Index data: 0 - 90	Middle data: 0 - 90	Ring data: 0 - 90	Pinky data: 0 – 90	Set multiple fingers Thumb ad/ab
Hand	1	Choose a finger to calibrate: 0 – not choose; 1 – choose					Open direction
Hand	2						Close direction
Wrist	4	Left actuator: 1 – up; 2 - down	Right actuator: 1 – up; 2 – down	Rotator: 1 – left; 2 – right	0	0	Calibrate wrist
Hand	5	0	0	0	Thumb: 1 – flex; 2 – extend	0	Calibrate thumb f/e
Elbow	3	1 – up; 2 - down	0	0	0	0	Calibrate elbow

Table 5: Serial packet format and value

Expanding number of choices for any modes or increasing the number of modes is feasible by applying similar packet structure to the new function in the controlled side and increase one or more control option in the controlling side, which is the main controller and watchdog timer. For mode 0, within the controller, there are the default hand figures of:

Figure name	Packet	Usage
Home all fingers	[0, 120, 0, 0, 0, 0]	Home all the fingers from the current position
Greek figure	[0, 120, 20, 40, 60, 80]	Offset all fingers by 20 steps for testing
Hold bottle	[0, 45, 80, 80, 80, 80]	Hand figure to hold bottle
Hold bag	[0, 45, 60, 60, 60, 60]	Hand figure to hold on to bag handle
Point finger	[0, 45, 0, 80, 80, 80]	Hand figure that points out the index finger: pressing doorbell or elevator
Hold pen	[0, 80, 60, 60, 80, 80]	Hand figure to hold a pen
Type 1 finger	[0, 45, 40, 80, 80, 80]	Hand figure to curl all fingers in and half-curl index finger for typing

Table 6: Default hand figure packet in controller

For I2C communication, the address is 0x01, 0x02, and 0x03 with respect to hand module, wrist module and elbow module. The packet is simply a structure of a character array of length 20 and a counter integer to keep track of the number of packets sent for debugging and for checksum purpose.

Within all controllers there are serial buffers, which read all packets sent and store. This is to ensure that all commands will be received and processed.

6.2. Brain-computer interface

6.2.1. Headwear

The project has implemented the design of OpenBCI [25] headwear as a general solution to support evaluation purpose. The headwear is divided into two parts of anterior and posterior. This is to allow the headwear to be printed with most commercial 3D printers. The parts of the headwear used are shown below:

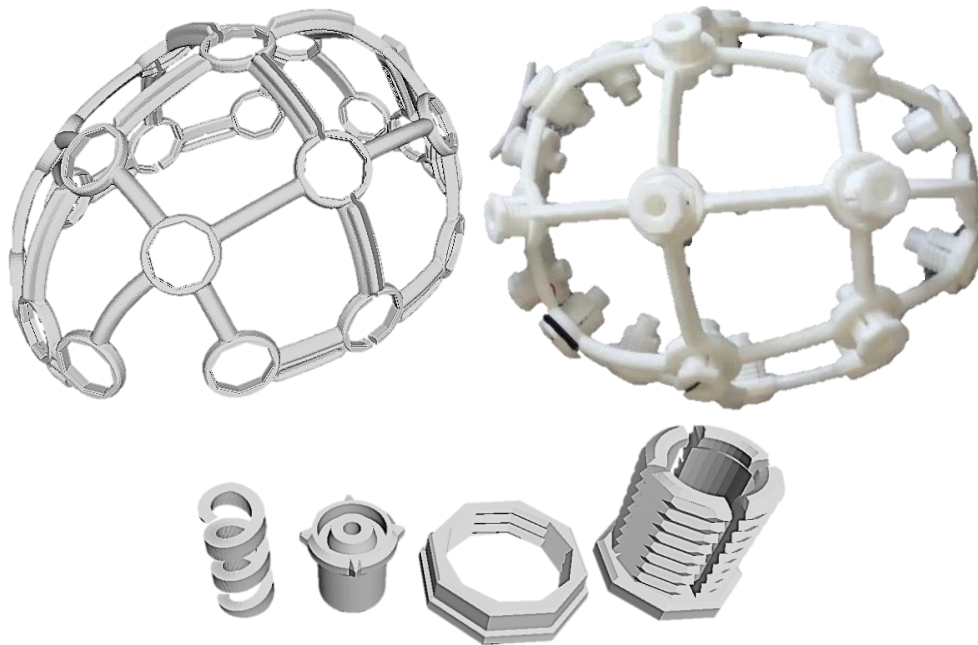


Figure 29: EEG headwear and electrode spring-loaded mechanism

The headwear follows the 10 – 20 system for BCI [18] and is 3D printed to the custom user head size. There are 21 locations to position electrodes. Each electrode is a spring-loaded module with parts indicated in the above figure. Due to the spring-loaded mechanism and the threaded installation, the electrodes could be positioned once on the first session, then be used for all other sessions without having to re-position. If the connection is loose or the contact point is not enough for measuring, the electrodes could be jiggled and lightly pressed inward to get closer to the scalp and sweep away the hair.

The use of right-leg driver (DRL) in BCI and EEG can increase the common-mode rejection ratio (CMRR) of analog circuit and thus be implemented. For this project, user ear lobe potential is used as DRL and an ear clip is demanded for the task. As medical grade ear clip for EEG practice is expensive, the ear clip is designed and manufactured using 3D printer and PLA, a medical grade material [43]. For highest analog signal insulation, apart from the contact point of the electrode, the ear clip is fully 3D printed, even with 3D printed spring. With custom design 3D printed spring, the applied force on earlobe could also be customized to not hurt the user. The design and final ear clip are shown in the following figures:

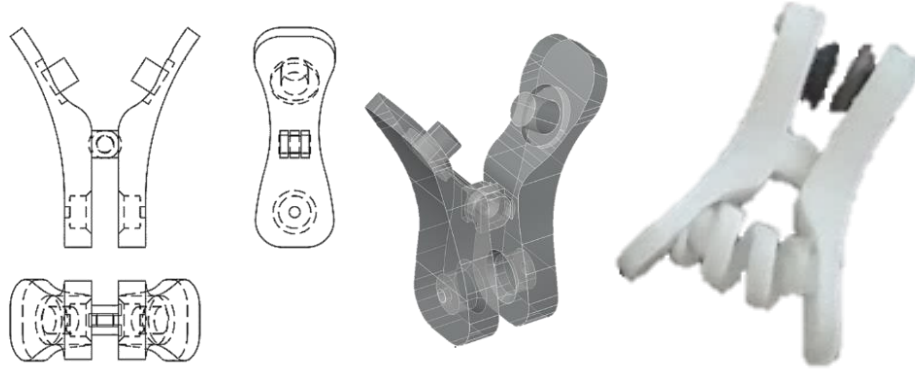


Figure 30: DRL ear clip design and printed

The used electrode is the medical grade dry and reusable electrode from Florida Research Instruments Inc. The datasheet provided by the manufacturer states that the following electrode could be reused for at least 20 times while maintaining high throughput characteristics and could even be disinfected for multiple uses. The electrode is composed of a conductive plastic and a coating of Ag/Cl. There is however a limiting factor that the coating could be removed through multiple attachments of the electrode lead. However, the use of this electrode in this project does not involve the use of electrode gel and attachment and detachment of lead, and thus the setup could be used for a sustainably long period.



Figure 31: Spike and no-spike reusable electrode for EEG

The headwear uses the spike electrode to get thought hair and acquire good contact with the human scalp surface. The ear clip uses the no-spike electrode to prevent causing pain and irritation.

6.2.2. BCI electronics

The final BCI electronics consists of multiple analog boards, with each board corresponds to an EEG channel, a digital board and a DAQ board for data acquisition. The boards are connected as shown in the following figure:

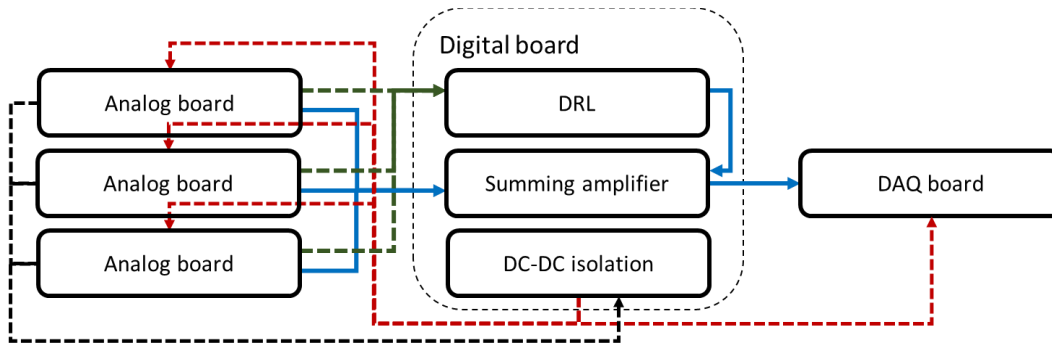


Figure 32: BCI modules interconnection

The analog board is responsible for amplifying and filtering the incoming EEG signal. The complete schematic of analog board could be found in [Appendix](#). The analog circuit is simplified into the following function blocks:

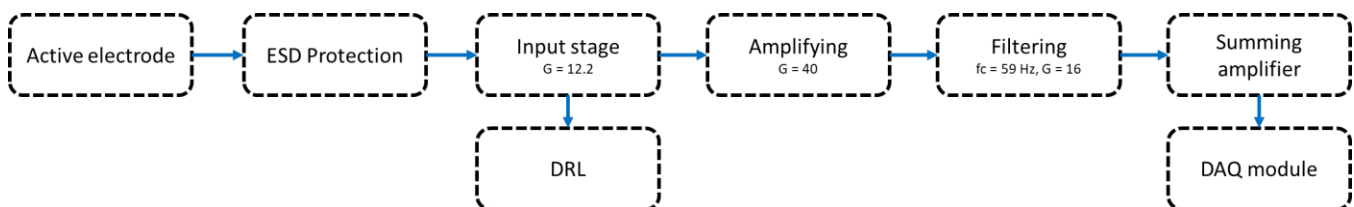


Figure 33: EEG analog circuit block diagram

The cumulative result is an EEG signal amplified 8000 times, cut-off at 59 Hz using 3rd order “Besselworth” filter. The input stage is a medical grade instrumental amplifier with high CMRR and high input impedance for lowest noise possible, even when being used with active electrode. The input stage is driven by DRL circuit, making the entire analog circuit float and that the virtual ground is always following the user electrical potential. The used instrumental amplifier is INA128, with several crucial features of having low offset voltage of 50 μV , high CMRR of 120 dB minimum, low quiescent current of 700 μA and is recommended for medical instrumentation and data acquisition applications.

The digital board is responsible for DC-DC isolation for general power supply, DC system power supply and analog circuit dual power supply. The digital board helps maintain 5V logic level across all modules. The digital board forwards signals coming from analog boards to DAQ board. The complete schematic of digital board could be found in [Appendix](#). The DAQ module is an Arduino Nano with built-in ADC and serial communication. The DAQ module receives power supply from the digital board discussed previously, samples the forwarded analog signals, processes packet and sends information out to other systems through serial communication. The DAQ module is designed as a shield for the digital board. The following figures show the final iteration of the discussed boards:

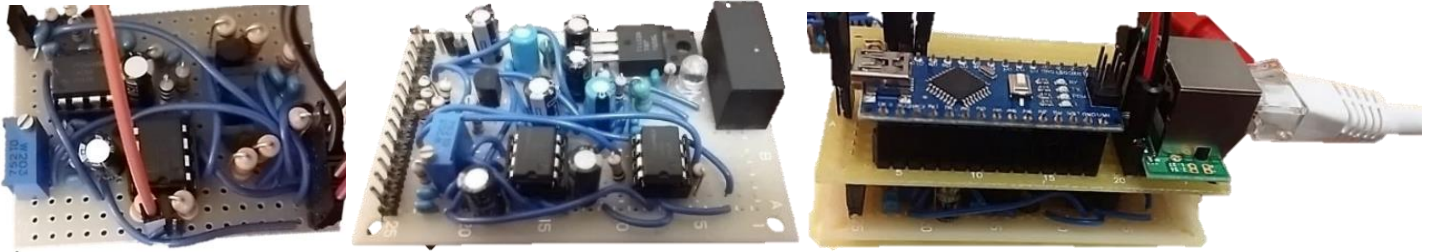


Figure 34: Analog board, digital board and DAQ board

To decrease the noise coming from the electrode to the analog circuit for data acquisition (DAQ) process, active electrode is used instead of passive one. Active electrode is basically a buffer circuit that utilizes the high impedance input of an operational amplifier to decrease incoming signal noise, buffer the signal, filter unwanted frequency if necessary, then pass a better signal to the next stage. The circuit for active electrode used is as followed:

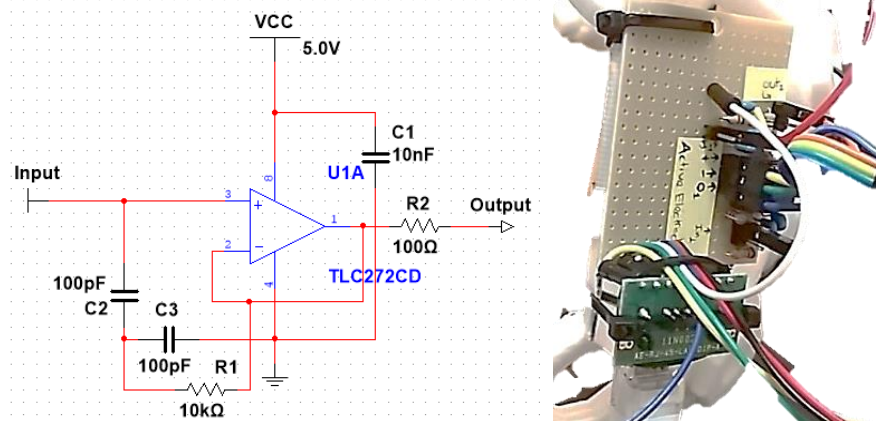


Figure 35: Active electrode schematic and implementation

The active electrode is placed as close as possible to the probing location to prevent signal from propagating too far from source. The PCB is installed at the back of the headwear and data is transmitted from active electrode to DAQ module using LAN cable. The system is tested with and without the use of active electrode. The result is drastically different, and it is derived through experiment that active electrode can eliminate most of 50 Hz humming noise from satellite electronic devices and preserve enough signal information for further analysis. The final headwear is shown below:



Figure 36: BCI final headwear

6.2.3. BCI firmware

Discrete Fourier transform (DFT) is used to analyze EEG signal. The discrete Fourier transform has the following equation [50]:

$$X[k] = \sum_{n=0}^{N-1} x[n]e^{-\frac{2j\pi kn}{N}}$$

With $X[k]$ is the k^{th} harmonic and $x[n]$ is the n^{th} input sample. Using the equation, the amplitude of respective frequency band could be calculated. For the DAQ board, the serial communication is done at baud rate 115200. Throughout the project, the sample rate for data acquisition has been constantly tested to find the optimal solution. Given the highest interested frequency following the project scope is 50 Hz, the sampling frequency must be higher than 100 Hz. On the other hand, the Arduino Nano only has 2 KB of SRAM and thus could only store a small buffer array before sending out through serial connection. These constraints suggest a speed – accuracy trade-off when choosing the final sampling frequency, as EEG signal must be sampled continuously for a long period before giving a visible and usable spectral information. A 14 Hz pulse signal is used to test the DAQ function of BCI. The first serial protocol used is shown below:

Start character	Counter	Data Array	Stop character
0x53	uint8_t	uint16_t [500]	0x45

The packet is sampled at 1024 Hz and stored in a buffer of 500 16-bit data-points in the module RAM before being sent out through serial. This method has proven to be insufficient for further spectral analysis of the acquired signal as the number of data-points is 500, with a sampling rate of 1024 Hz, only gives out a window of 488.3 milliseconds. Yet the amount of time for the DAQ software to acquire the packet and get ready to read the next packet will cause pulses of delay across the signal and thus lower the credibility of spectral analysis. With a packet size of 500 and sampling frequency of 1024 Hz, discrete Fourier transform could be applied to find amplitude of frequency band, following the equation below:

$$n = \frac{N}{F_s} \times f$$

With n is the index of the calculated harmonic array of discrete Fourier transform, N is the packet size, F_s is the sampling frequency and f is the frequency of interest. Following this equation, if only the frequency band of 0 – 50 Hz is interested, only the index from 0 to 24 ($500 \times 50 / 1024$) of the harmonic array must be used. The equation also shows the effect of packet size and sample frequency on the resolution of DFT result. The following figure shows the effect on the FFT result of a 14 Hz pulse signal:

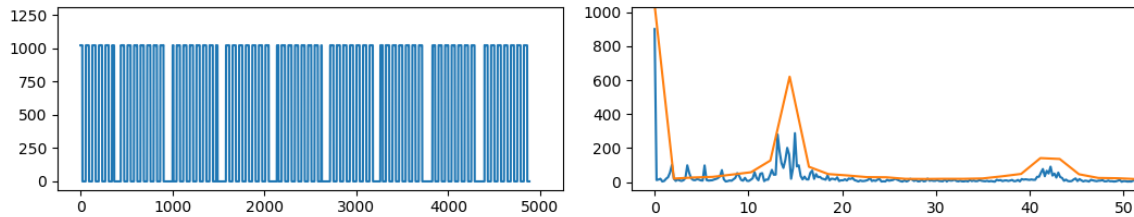


Figure 37: Effect of delay pulses on FFT analysis

The figure shows time domain plot put aside the frequency domain plot. The time domain shows small gaps of blank data between large groups of blue signals (a packet). The frequency plot shows two lines, with the orange line is FFT analysis on one packet and blue line is FFT analysis on a buffer of 10 packets. As the signal created is a 14 Hz pulse wave, it is expected that FFT analysis should show similar result, with the first harmonic frequency at 14 Hz. Although the orange line peaks at 14 Hz, the blue line is attenuated and could not peak at 14 Hz due to the result of blank pulses. This is a critical problem as EEG analysis focuses on different brain rhythms with unique frequencies and is conducted on a window between several hundreds of milliseconds to 10 seconds [14, 20-23]. This suggests an alternative sampling frequency and serial protocol. The new serial protocol is designed, and the new packet design is shown below:

Start character	Counter	Data Array	Stop character
0x53	uint8_t	Uin8_t [1500]	0x45

The data is sampled at 256 Hz, instead of 1024 Hz. As seen from the packet design, the data is quantized at 8 bits instead of 10 bits. The use of 10-bit ADC causes 6 bits redundancy in every data point of the packet (as the data points must be encoded as either 8-bit or 16-bit integer) and through practical implementation, the EEG signal acquired from DAQ module almost never surpasses 255. Thus, each data point could be encoded using 8-bit integer. Subsequently, the packet size will also be increased, from 500 to 1500 effectively. The 1500-point packet, being sampled at 256 Hz, gives out a window of almost 6 seconds. In case of multiple channels used, the 1500 points in each packet could be divided by the number of used channels to send out information of all channels at once. Given the methodology applied, 2 channels could be used to acquire EEG signal and subsequently, a divided window of 3 seconds is still enough to provide accurate spectral analysis.

Using this new packet design, the harmonic resolution is $256/1500 = 0.1706$ Hz, which is better than the first design. However, this design only sends a packet at every 5.8 seconds (1500 points/256 Hz), the DAQ module will lose its real-time view and has proven to be hard to debug and/or conduct test on. A solution is thus made to address this problem, that is instead of logging a packet out immediately after it is acquired, it is better to phase shift all packets with 1 packet, and gradually output the data points as if the data is sampled in real-time. Doing so helps the user to see the signal flow and gives out a sense of real-time implementation. This method, though overcomes the need for real-time viewing, will still output data that is sampled approximately 6 seconds ago (effectively 1 packet shift). Yet eventually all data points will still be collected with correct timestamp with respect to each other and thus the post-sampling analysis process will remain credible and accurate.

The software is tested with a record of 14 Hz pulse signal again. The new FFT analysis shows correct result of 14 Hz peaking sharply, with the second harmonic frequency for pulse signal at $14 * 3 = 42$ Hz. The FFT is accurately calculated and shown, without having any attenuation as of in the previous version. On the other hand, using the same function on a long signal of 14 Hz pulse, changing the window size shows the corresponding changes in the FFT analysis, and consequently this proves the accuracy of the developed FFT function. The test result is shown in the following figures:

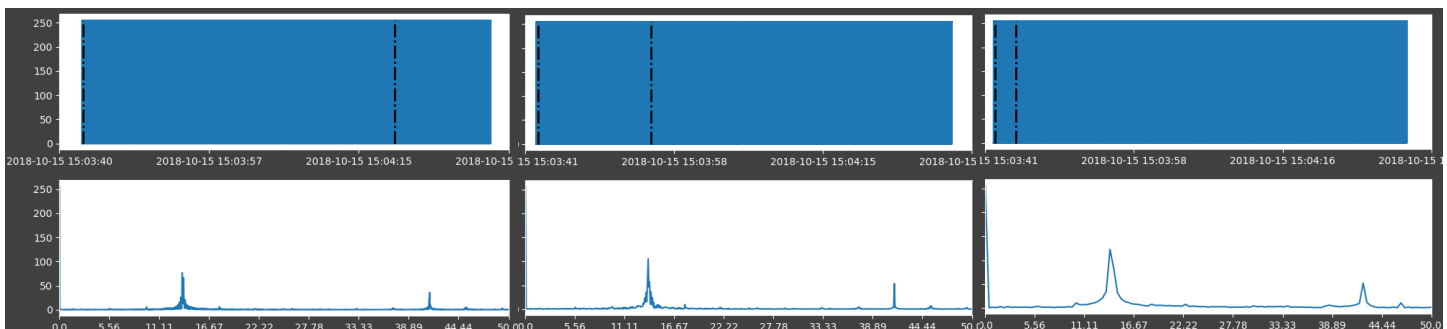


Figure 38: FFT function credibility test with 10-second, 5-second and 2-second window

The three figures show the credibility test result of FFT function. FFT is applied on the same 14 Hz pulse signal, with different window sizes. The window is shown by the left and right black dashed lines on the time domain plot, and following the reversed order of the figures, the larger the window size, the more accurate and sharper the FFT analysis becomes. This has drawn out two important conclusions: the new packet design gives good FFT analysis result; and the FFT function of the DAQ software works correctly. This DAQ software is then used to acquire EEG signal with higher assurance.

Thus, the final serial protocol used is 256 Hz sampling rate, with a serial buffer of 1500 single-byte data points for 1 channel, or two buffers of 750 single-byte data points for 2 channels. The following figures show the final BCI with two channels running concurrently:

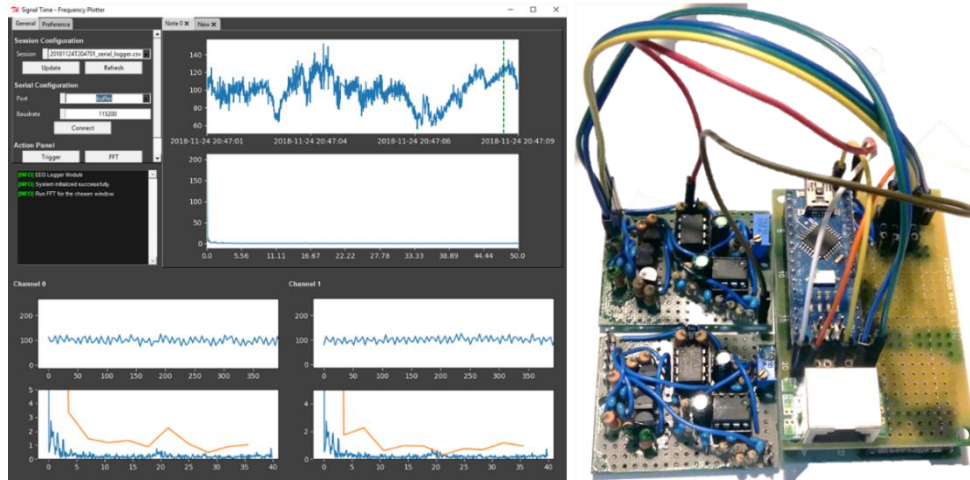


Figure 39: Dual-channel BCI – software and hardware

6.2.4. BCI functions

As the electronics and the data acquisition of BCI have been tested and proven usable, EEG alpha trigger test is conducted. Alpha wave mainly originates from occipital lobe when subject is awake and relax with eyes closed. Alpha wave is suppressed when subject opens eyes, or experiences drowsiness or sleepiness [13]. On the other hand, when subject is awake and conscious, beta wave is usually found [13]. From these statements, alpha wave could be recorded if subject closes eyes and beta wave could later be observed when subject opens eyes. The following figure shows beta and alpha brain rhythm recorded by using the designed BCI with electrode positioned at C4 – P4 pair:

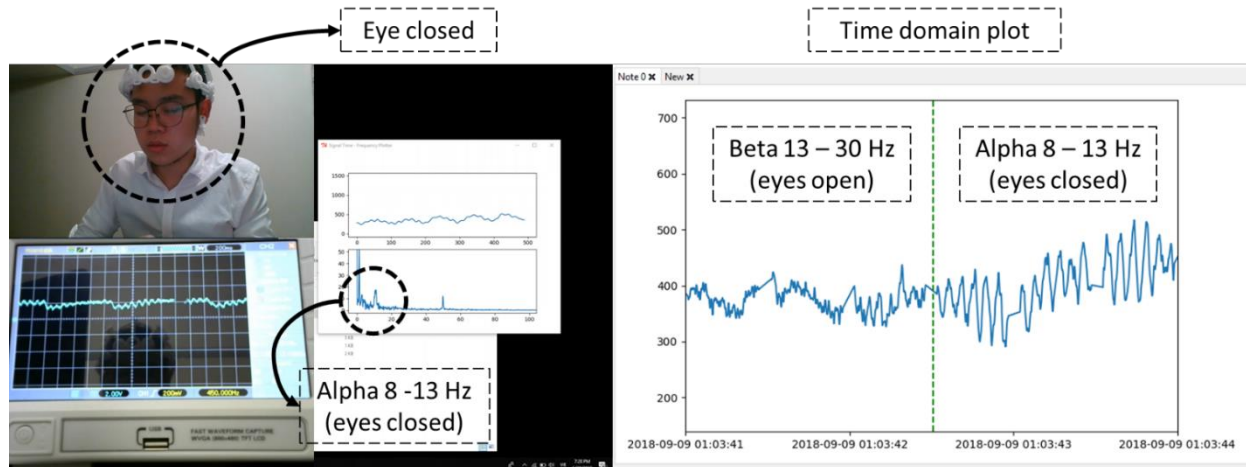


Figure 40: Alpha trigger test recorded using designed BCI

The success of alpha trigger test proves that the designed BCI could be used for EEG acquisition, and that this phenomenon could also be used as one input channel for the prosthesis. Using the provided DFT equation, the amplitude of only the alpha band could be calculated and used to trigger the system. The harmonic array index is calculated as followed:

$$\min = \frac{1500}{256} \times 8 = 46.8; \max = \frac{1500}{256} \times 13 = 76.17$$

As EEG signal is sampled and calculated using a 1500-data point window, it is considered a non-periodic energy signal. Thus, the energy of the alpha band could be calculated as followed:

$$E = \sum_{n=min}^{max} X[n]^2$$

With $X[n]$ is the harmonic array calculated using DFT, and max, min are calculated above. Similar method is applied for the second test of SSVEP, with four visual stimuli of 10, 15, 20, 25 Hz. The stimuli are LEDs being controlled through timer interrupt to blink at the chosen frequencies. It is important to address that if the stimulus is to create a 10 Hz visual trigger, it must be controlled with a 20 Hz interrupt. The following figures show the SSVEP test result, with each stimulus recorded for 60 seconds:

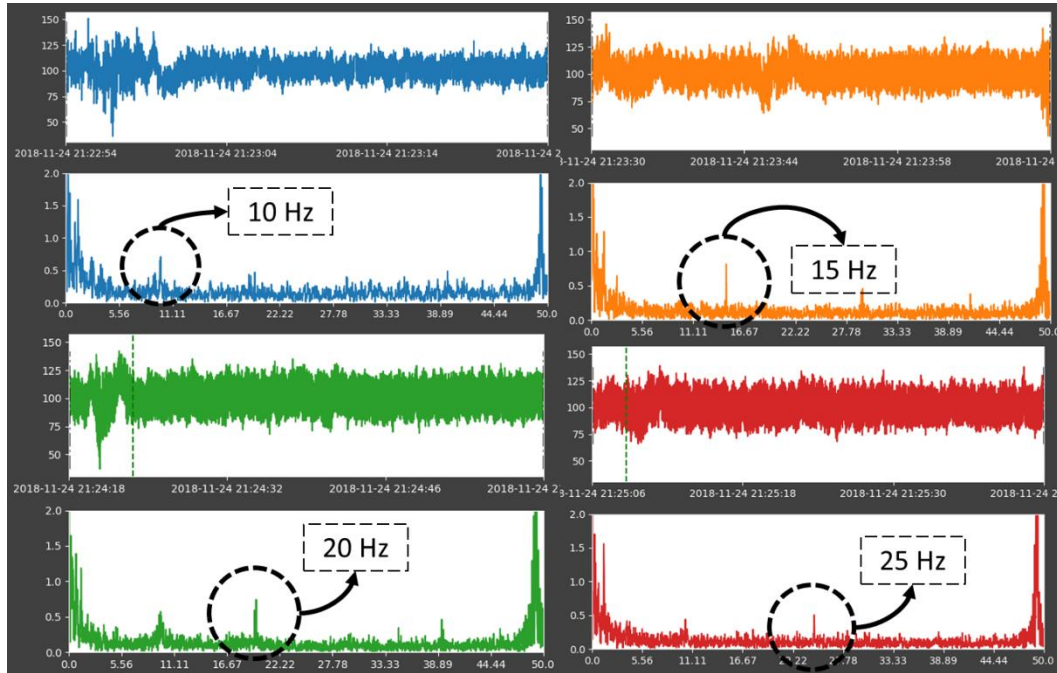


Figure 41: SSVEP test result - 10 Hz (blue), 15 Hz (orange), 20 Hz (green) and 25 Hz (red)

From the peaks in four frequency plots, it is derived that SSVEP test is successful, and that SSVEP could be used to control the prosthesis, given an appropriate control scheme. However, the test is conducted with 60-second window, which is not an optimal response time for a real time system. The energy for the frequency bands of SSVEP is calculated using similar method applied to alpha band. The energy of 60-second signal is used as threshold value for each band. The system is designed to then calculate energy of the 4 bands of SSVEP whenever new signal is received, and if the new energy is higher than threshold value, the system executes an action assigned to that band. To further improve SSVEP, the signals from multiple packets are merged and calculated. The system is then benchmarked by playing a simple 2D game shown below:

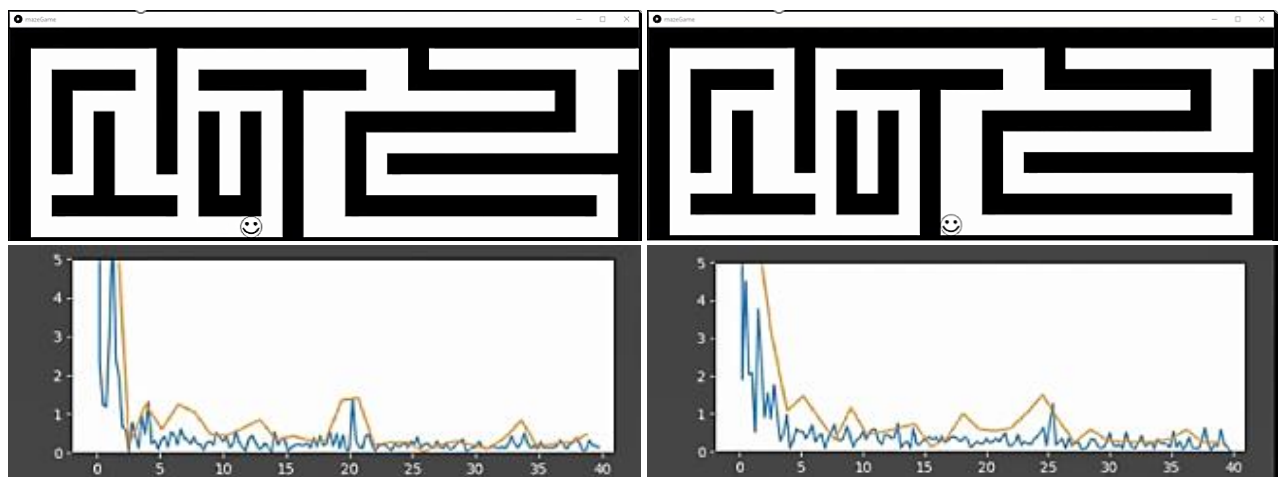


Figure 42: SSVEP maze test - signal view with 20 Hz trigger (left) and 25 Hz trigger (right)

The test conducted is a simple maze game controlled using SSVEP, with up, left, right and down correspond to 10, 15, 20 and 25 Hz. The result is promising, with the BCI detecting the stimulus after an average of 5 seconds. This suggests that SSVEP is responsive enough to be used in real time application.

6.3. Hybrid active vision system

The object recognition model is trained using TensorFlow and 20-COCO-based objects [34]. The algorithm used to train the model is MobileNet SSD as stated in literature review. 20 random objects are chosen from COCO dataset: airplane, bicycle, bird, boat, bottle, bus, car, cat, chair, cow, dining table, dog, horse, motorbike, person, plant pot, sheep, sofa, train and television monitor. The images are labelled and used to train. The following figures show the training and evaluating process:

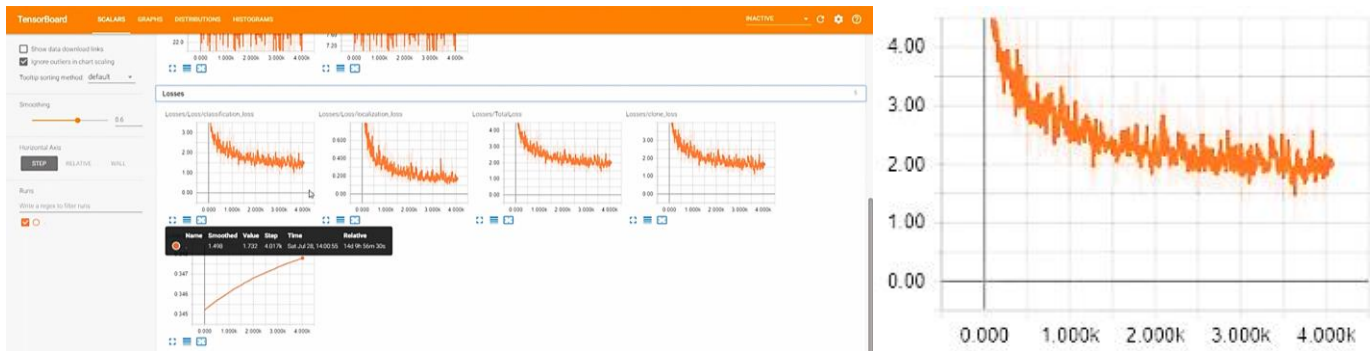


Figure 43: Training total loss after 4000 steps – TensorBoard view and detailed graph view



Figure 44: Evaluation image after 1500 steps

Figure 45: Evaluation image after 2500 steps

Figure 46: Evaluation image after 3500 steps

The evaluation process shows the bottles gradually recognized by the model. After 4000 steps, the model training process is finished and is then deployed on three different models of Raspberry Pi of 3B+, 2B+ and Zero W. The following figure and table show the result of the deployment:

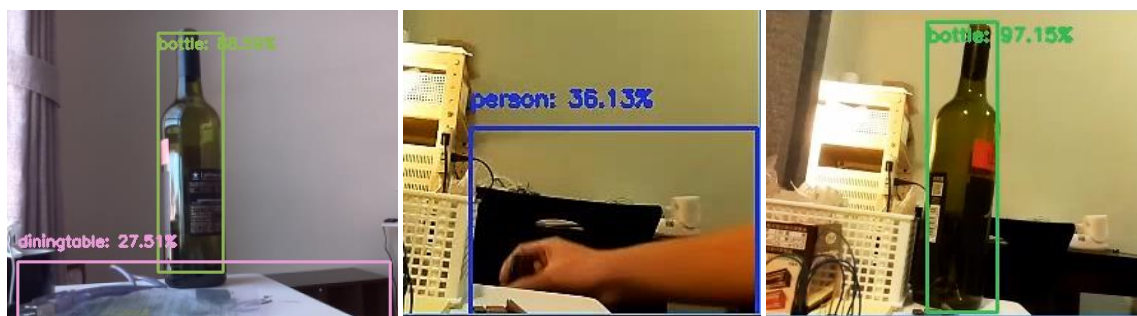


Figure 47: Model deployment on Raspberry Pi

Model	Raspberry Pi Zero W	Raspberry Pi 2B+	Raspberry Pi 3B+
CPU	1 GHz	900 MHz	1.4 GHz
RAM	512 MB	1 GB	1 GB LPDDR2 SDRAM
Runtime	0.1 FPS	0.5 FPS	1.2 FPS

Table 7: Different raspberry pi models CV performance comparison

The result is insufficient for real-time application and considering alternative options for both hardware and software, the used Pi models are among the best options on the market in terms of speed and cost; and the used algorithm for object classifier, MobileNet SSD, has proven to be the best option as it has the highest mean average precision (mAP) among the algorithms designed for real-

time processing application [36]. It is thus important to apply new methodology and/or engineering approach for the current problem, rather than improving solely either or both in hardware and software.

A novel method is applied to support the previous method used for computer vision. Instead of running object classifier at every iteration, which is proven to be resource consuming and put heavy computational stress on the system, the object classifier will be run until the object of interest is acquired and locked into view. It is then object tracker will be used in place of object classifier. OpenCV supports 7 different tracking algorithms, namely be boosting, MIL (Multiple Instance Learning), KCF (Kernelized Correlation Filters), TLD (Tracking, Learning and Detection), Median Flow, GOTURN, MOSSE (Minimum Output Sum of Squared Error) and CSRT (Discriminative Correlation Filter with Channel and Spatial Reliability). All 7 trackers are practically tested using different videos and live camera actions, from which the results are acquired and recorded into the following table:

Tracker	Average FPS	Note
CSRT	20	Highly accurate Could not scale with the object
KCF	45	Lose track easily
Boosting	15	Re-track when object falls back in current tracker
MIL	12	Lose track easily, could not re-track
TLD	17	Scale with the object size Tracker fluctuates too much
Median Flow	160	Scale with the object size Lose track with fast movement
MOSSE	245	Could not track at all and/or lose track easily

Table 8: Different tracker comparison

As it is proposed that CV will be used when the user moves closer to the object, detects the object and chooses a grip pattern, the tracker must be able to scale with the object size, as the closer the user gets to the object, the larger the size of the object becomes on the CV viewpoint. It is thus only two options left, namely be TLD and Median Flow. On the other hand, Median Flow has fast computing speed, peaking the test at 160 FPS. Hence, Median Flow is chosen as the tracker algorithm to be used with the CV module. In addition to this practical test, Median Flow is also found from literature research to be highly robust and fail-safe.

As a tracker module is introduced to the system, and given the increment in the wrist DOF, EEG and EMG cumulatively do not provide enough input to control all the mechanical module. Thus, another approach is introduced, that is to use the tracker with the wrist module, calibrates the wrist to always positions the object at the center of the palm based on the relative position of the object on frame captured by CV. Tracker will be used to acquire the coordinate of the object with respect to the frame, calculate the offsets between the tracked location and the center of the frame, and feedback the corresponding data to the wrist module.

To test the approach without damaging the mechanical arm, a quick implementation of the tracking – centralizing method is first done on a simple pan-tilt robotic frame. The active vision system will move the camera according to the movement of the object so that the center of the tracking bounding box will always be at the center of the camera frame. A PID model is implemented on the offset x and y of the bounding box center and the frame center. To address problem with saccade movement, a delay is introduced to the control loop that is proportional to the calibrated value of the motors. A threshold is also applied on the control system as to maintain the system overall stability. This is due to the low resolution of the used servo motors, which only has the resolution of 1 degree. The PID model is fine-tuned using Ziegler-Nichols method. The follow equation set shows the final control model of the active vision system:

$$a_x = d_x = \begin{cases} 0 & \text{if } x_0 < 0.005 \times \frac{W}{w} \\ 0.065 \times x_0 \times \left| \frac{x_0}{x_1} \right| & \text{if } x_0 \geq 0.005 \times \frac{W}{w} \end{cases}, \quad a_y = d_y = \begin{cases} 0 & \text{if } y_0 < 0.005 \times \frac{H}{h} \\ 0.05 \times y_0 \times \left| \frac{y_0}{y_1} \right| & \text{if } y_0 \geq 0.005 \times \frac{H}{h} \end{cases}$$

With the following variables:

- a_x, a_y : The calibrated angle value for x and y
- d_x, d_y : The delay applied onto the iteration
- x_0, y_0 : Current offset pair
- x_1, y_1 : Previous offset pair
- W, H : Width and height of the frame
- w, h : width and height of tracker rectangle

The scaling factor of Median Flow is also used to compute the relative position of the object in three-dimensional space. This is to determine if the object is moving further away or closer to the vision system. The final system is tested using actual objects which

are included in the detection model. For the simplicity of the test, the class “person” is omitted so that the system will only detect the object of interest. The following figures show an actual test of the system, the object used is a bottle:



Figure 48: Pan-tilt module with tracker test

The figures are extracted from a recorded test of the system in action. The capture interval between figures are 500 milliseconds. The bottle is moved around the test area with different constant speed and different random acceleration. The overall system could successfully follow the object even when the object is moved 40 m/s, 1 meter away from the camera (angular speed of 75 degree per second).

When the object is moved slowly, the blob bounded by the tracker rectangle is fed into object detection model to check for tracking failure or to rebound the object with a more accurate bounder. The object detection and object tracker are complementary, and the gain is proportional to the error. This means that if the object is stationed, majority of resource is used for object detection and if the object is moved, object tracking has higher priority.

The test shows feasibility in using this approach to further control the wrist and increase the overall system robustness. On the other hand, as of the performance of the CV module, using the hybrid system of object classifier – tracker module on different Raspberry Pi models shows a vast increment in FPS:

Model	Raspberry Pi Zero W	Raspberry Pi 2B+	Raspberry Pi 3B+
Object classifier	0.1 FPS	0.5 FPS	1.2 FPS
Object classifier - tracker	5 FPS	12 FPS	20 FPS

Table 9: New CV model performance comparison

The hybrid active vision is usable for real time application. However, to further improve the runtime, a cloud server is added into the system to support the heavy computational processes. When the system obtains a network connection, it will try to call for the cloud server. When a connection is established, the system will start sending the fetched images from camera to the server. The server will then run object recognition, object tracking and response with control information that will in turn calibrate the pan-tilt frame. This set up is tested on similar Pi models and the result is promising:

Model	Raspberry Pi Zero W	Raspberry Pi 2B+	Raspberry Pi 3B+
Object classifier	0.1 FPS	0.5 FPS	1.2 FPS
Hybrid system	5 FPS	12 FPS	20 FPS
Hybrid system + cloud	10 FPS	20 FPS	30 FPS

Table 10: New CV system with cloud server performance comparison

The system can run active vision seamlessly on all hardware. With this achievement, the mechanical arm can be controlled using only Raspberry Pi Zero W, which is not only the smallest model but also the least expensive among the three. With all the test cases finalized, the pan-tilt robotic frame is replaced with the actual mechanical frame, and the result is shown below:



Figure 49: Hybrid vision with cloud - test on mechanical arm - side view

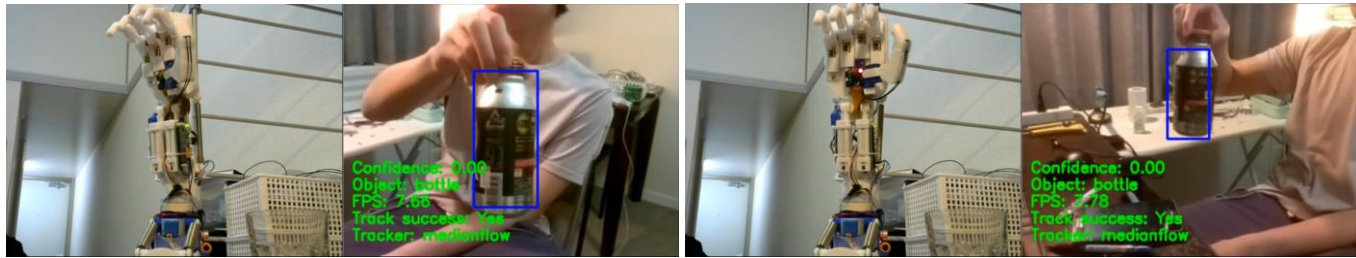


Figure 50: Hybrid vision with cloud - test on mechanical arm – front view

The figures are captured from footage of a real test. The system successfully tracked the bottle, checked for object credibility while maintaining an average of 10 FPS. The system can run both online and offline, with an average of 5 FPS when offline and 10 FPS when online. The system could switch from one mode to another to eventually obtain the best runtime possible. With the cloud server, new object recognition models could also be deployed, or tested without causing critical errors on the main system.

6.4. EMG sensor and elbow control

The EMG sensor is designed from the early stage of the project and is a simple analog circuit consisting three stages of input, amplification and rectification before fetching the output pulse to an ADC. The EMG schematic and PCB is shown below:

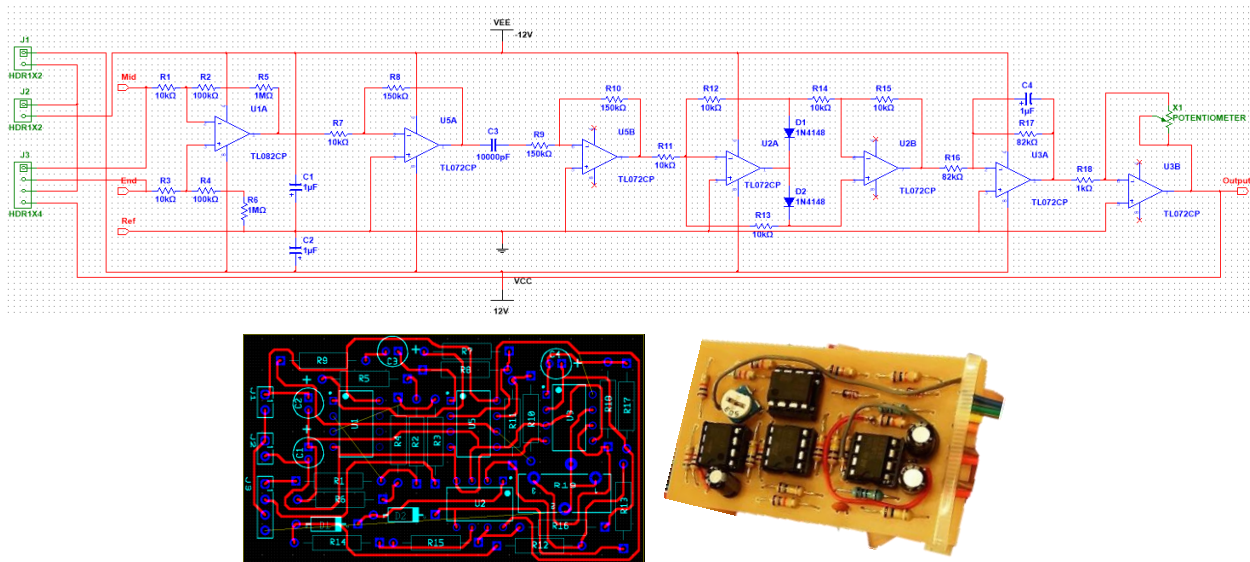


Figure 51: EMG schematic and PCB 1-layer design

The EMG sensor design has been tested on 10 individuals and a patient suffering from congenital limb defects. All participants are voluntary, informed about the test priory, with acknowledgement of the components used and the methodology used. Throughout the test, applied current level to EMG sensor is monitored using industrial grade instruments and is kept as safety level. All participants show good result from the first trial of the sensor and able to freely control a linear 3-bit ADC system. A sample control model for elbow module is proposed as followed, based on the 3-bit output of the ADC system when muscle is flexed:

Action level	Interpretation	Action
Below 3, hold for 2 seconds	Elbow module	Move elbow downward 1 step
Above 5, hold for 2 seconds		Move elbow upward 1 step
Pulse above 4	BCI system	Start/stop SSVEP
Double pulses above 4	Wrist module	Start/stop CV module

Table 11: EMG action mapper

The EMG control scheme enables executive interrupt from user when problem arises to other modules.

6.5. Final distributed system

The mechanical arm V2, the BCI and active vision system are combined. SSVEP could be used to choose the target module to be controlled by either EMG or alpha trigger. With different combination of SSVEP triggered channels, EMG and alpha trigger, several control schemes could be proposed, and the users could choose the scheme they find the most comfortable and intuitive to use. A

sample scheme currently being used is EMG for elbow movement, alpha trigger for hand module open/close and active vision system for wrist movement. The following figure shows the entire system in action:

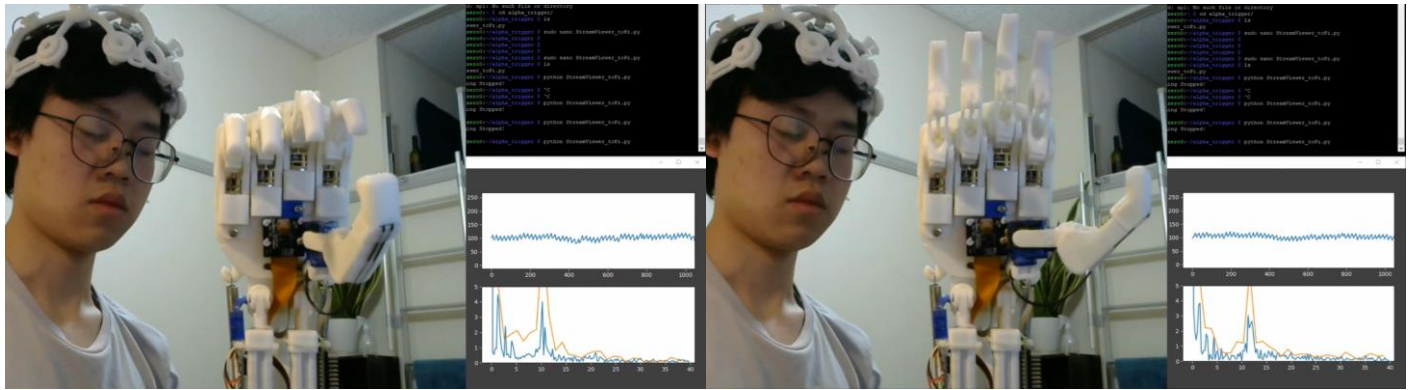


Figure 52: Alpha trigger targeting hand module

With alpha trigger assigned to hand module, the frame captured by the camera is rotated 90 degrees, pan-tilt configuration is switched to tilt-pan configuration, the prosthesis can track the object with the hybrid system and user could choose when to close the hand to pick up the object. The vision system also checks for the relative distance between the palm and the object, so that even if the user is falsely creating alpha signal, the hand will not close, or will only close when the object is close enough to be picked up.

To maintain the system stability, when the object has been found and user has triggered the arm to grab the object, the vision system will be terminated and will only be turned on again when the hand module is triggered to open again. This is to also provide the camera with the widest view angle and is not blocked by objects, or any fingers. The entire process from approaching object, to positioning palm and grabbing object at will is shown in the following figures:

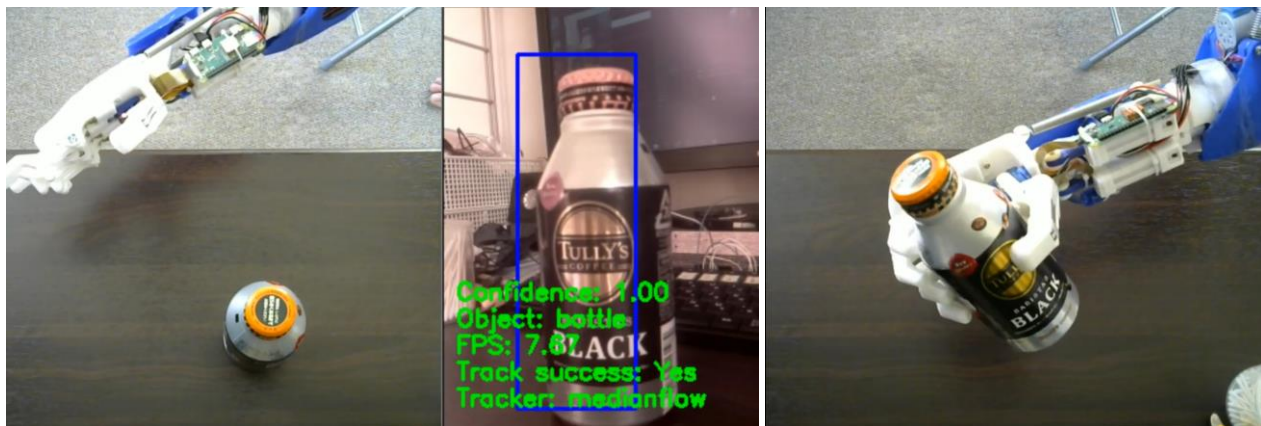


Figure 53: Hybrid active vision targeting object and picking object up

The entire system is functional, concurrently running and sharing resources from one to another. The system offers numerous control possibilities that user could choose from and pick the most intuitive one to use.

6.6. User application

To further support user with post-assembly upgrade and maintenance, an application is developed that allows user to visually assign new hand grip patterns to the system. The application is an animated arm that takes input from a virtual socket and change the hand figure on screen in real-time and finger curl angles accordingly. The software is based on Java with 3D arm parts designed with AutoCAD and imported in as 3D objects. Each part is defined with pivot location, rotate location and offset between rotate location and base point. Using these information, individual parts can be controlled accordingly. There is also a Python medium and a serial connection to communicate with the hand module through standard pre-defined serial packet. The animated arm joints could be controlled using mouse click and mouse drag events, then a packet of arm joint information is sent to the Python medium using virtual socket. The Python medium then re-formats the packet and forwards it to the hand module. The following figure shows the driver in action:

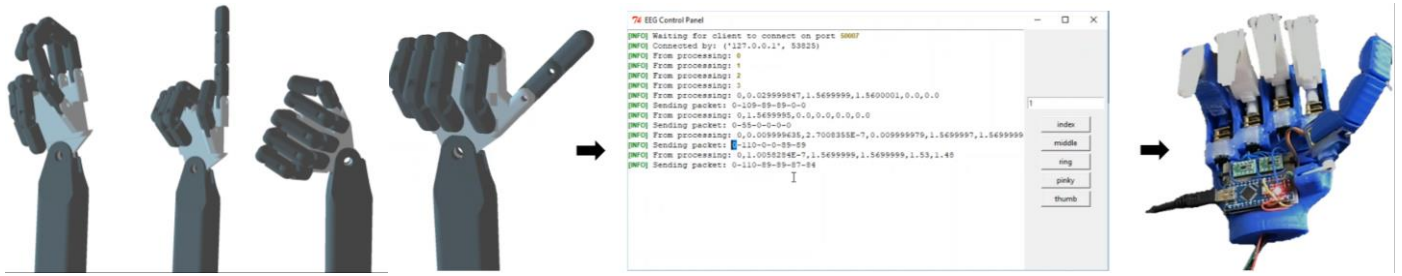


Figure 54: Sample hand patterns and end-user application for customization and debugging

Using this application, the user could interact with the animated hand on computer to create new hand grip patterns, which will then be transferred into the mechanical arm and stored as a set of customized patterns, which could then be called out while user is using the prosthesis. The application enables personalization, and thus opens new possibilities and increases system overall scalability.

7. Project management

7.1. Time management and Work Breakdown Structure

The following figure shows a figure obtained from the used Gantt chart for project management of the entire system, with a focus to January 2019. The overall completion percentage of the project is **92.13 %**. This is due to the narrow of manufacturing PCB scopes to lower the project cost. However, other scopes are expanded during the project, including the addition of SSVEP, new mechanical arm design (V2) with more DOF than V1, and hybrid active vision system.

EEG PROSTHESIS - WBS AND GANTT 2018	Start day	End day	Duration	Responsibility	Percentage																	
	6/25/2018	2/15/2019	235	Nguyen Phuong Duy Pham Chi Thanh	92.13	4-Jan	5-Jan	6-Jan	7-Jan	8-Jan	9-Jan	10-Jan	11-Jan	12-Jan	13-Jan	14-Jan	15-Jan	16-Jan	17-Jan	18-Jan	19-Jan	
Design modular EEG with 1 channel	7/1/2018	7/15/2018	14		100.00																	
Design modular EEG with multiple channels	7/15/2018	8/15/2018	31		100.00																	
Test signal processing	8/15/2018	9/15/2018	31		100.00																	
Packet design for serial transmission	7/15/2018	7/18/2018	3		100.00																	
PCB design	9/1/2018	10/15/2018	44		100.00																	
Computer vision	6/25/2018	9/1/2018	68		100.00																	
Using DNN packet of OpenCV for preliminary testing	6/25/2018	7/15/2018	20		100.00																	
Use pre-made models and deploy to Pi	7/15/2018	7/25/2018	10		100.00																	
Collect database and train own model for 1 object	7/20/2018	7/30/2018	10		100.00																	
Multiple objects segmentation and classification	8/1/2018	9/1/2018	31		100.00																	
Mechanical arm	8/1/2018	2/15/2019	198		97.16																	
Working with Arduino	8/1/2018	10/1/2018	61		100.00																	
Hand design individual fingers and thumb	8/1/2018	8/15/2018	14		100.00																	
Wrist and elbow design	8/15/2018	8/25/2018	10		100.00																	
Test EMG on moving elbow	9/1/2018	9/8/2018	7		100.00																	
Test EMG on switching hand figure	9/8/2018	9/15/2018	7		100.00																	
Test EMG on elbow, button interface for hand figure	9/15/2018	10/1/2018	16		100.00																	
Working with Pi and Arduino for sub-modules	10/1/2018	2/15/2019	137	Nguyen Phuong Duy Pham Chi Thanh	93.75																	
Test EMG on elbow, computer vision for hand figure	10/1/2018	11/1/2018	31		100.00																	
Test EMG on hand open/close, EEG for elbow, camera vision for hand figure	11/1/2018	12/1/2018	30		100.00																	
Test EMG on hand open/close, EEG for elbow, camera to support hand figure	12/1/2018	1/15/2019	45		100.00																	
Test EEG on all arm, EMG and computer vision to support filtering EEG signal	1/15/2019	2/15/2019	31		75.00																	
Advance Design	10/15/2018	12/15/2018	61		92.22																	
Mechanical arm	10/15/2018	11/30/2018	46		100.00																	
New mechanical finger design with encoder	10/15/2018	10/20/2018	5		100.00																	
New thumb design with 2 DOF	10/20/2018	10/30/2018	10		100.00																	
New linear actuator design with encoder	10/25/2018	11/5/2018	11		100.00																	
New wrist design with 3 DOF	11/1/2018	11/15/2018	14		100.00																	
New forearm design with battery slot	11/15/2018	11/25/2018	10		100.00																	
New spring-loaded elbow design	11/20/2018	11/30/2018	10		100.00																	
Computer vision	10/20/2018	12/1/2018	42		100.00																	
New object tracker module, vertical and horizontal track	10/20/2018	11/1/2018	12		100.00																	
New object tracker module, angular calibration	11/1/2018	11/15/2018	14		100.00																	
New object tracker module with new object detection on prosthesis	11/15/2018	12/1/2018	16		100.00																	
BCI	11/1/2018	12/15/2018	44		76.67																	
New EEG headwear design	11/1/2018	11/15/2018	14		80.00																	
Test SSVEP	11/10/2018	12/1/2018	21		100.00																	
Test SSVEP with motor imagery	12/1/2018	12/15/2018	14		50.00																	

Figure 55: Gantt chart for project management, starting November 2018 to December 2018

7.2. Cost management

The overall cost for the entire system is recalculated using information of both Japan market and Vietnam market. The entire system has an average cost of **180 USD**, roughly **4 million VND**. This price point has proven to be an adequate expense for prosthesis with respect to a research on Vietnam average income [51]. The following table shows the Bill of Materials of the system, which also takes in account the cost of PLA plastic for 3D printing:

name	Vietnam price (1,000 VND)	Initial price (1,000 VND)	Unit	quantity	Intial Price	Vietnam Price
arduino nano	70	70	piece	4	280	280
drv8835	40	40	piece	6	240	240
stepper motor 28BYJ-48	60	40	piece	1	40	60
raspberry pi zero w	640	300	piece	2	600	1280
camera module	350	400	piece	1	400	350
N20 motor	90	95	piece	8	760	720
servo motor SG90	35	40	piece	1	40	35
OLED I2C	95	95	piece	1	95	95
button	5	5	piece	2	10	10
INA128	97	90	piece	3	270	291
LMC6482	10	10	piece	9	90	90
BC547	2	2	piece	6	12	12
BC557	2	2	piece	6	12	12
MCW03-05S05 DC-DC	130	90	piece	1	90	130
220nF	1	1	piece	3	3	3
33nF	1	1	piece	3	3	3
1uF	1	1	piece	6	6	6
10pF	1	1	piece	3	3	3
100pF	1	1	piece	18	18	18
1nF	1	1	piece	9	9	9
10nF	1	1	piece	12	12	12
100nF	1	1	piece	18	18	18
47uF	1	1	piece	6	6	6
20k Potentiometer	2	2	piece	3	6	6
200 kOhm	10	10	pack	1	10	10
2.2 kOhm	10	10	pack	1	10	10
4.7 kOhm	10	10	pack	1	10	10
NJM 431	13	8	piece	1	8	13
2 cell serial charger	20	30	piece	1	30	20
18650 battery cell	65	65	piece	3	195	195
Step-down converter	16	15	piece	2	30	32
1-kilogram PLA filament	375	550	spool	1	550	375
PCB	5	5	piece	10	50	50
Ag/AgCl electrode	12	12 (0.50 USD converted)	piece	3	36	36
Total					3952	4440

Table 12: Cost analysis based on market research and purchase history

7.3. Risk management

The following table shows the risk management process of the project, which could later be used for troubleshooting:

Module	Sub-module	Hazard	Risk	Solution
EMG and EEG module	Electrode	Corrosion	High	Use medical grade electrode (Ag/AgCl).
		Rash and scratches	Medium	Use spring will small stiffness. To be used with impedance tester for optimal surface contact without applying too much force.
		Loss connection	High	Watchdog to reset system, impedance matching process to find connection loss
		Broken wires	High	
	MCU - Pi	Deadlock	Medium	System will not turn on and/or modules are self-maintained. Battery indicator to inform user to recharge.
		Insufficient power supply	Low	
	Serial connection	False packet format	Medium	Checksum for every packet sent
		Loss connection	High	Endpoint to immediately signal watchdog to inform user and power down entire system. Ready to reset.
		Deadlock endless loop	High	Counter in every packet to omit duplication.
	CMOS camera	Blurry	Low	Stop module and signal user

Computer vision module		Broken due to sharp objects to be held	Medium	Camera is hidden deep inside the palm and covered with a layer of transparent acrylic.
		Out of focus	Medium	Blur detection in computer vision function to detect and inform user to recalibrate or self-calibrate.
	MCU – Pi	System down due to excessive processing	Medium	Watchdog to reset system and log error
		Slow processing causes faulty calibration	Low	Object tracker to help object classifier. EMG module to support user trigger.
Mechanical arm module	Hand, wrist and elbow mechanics	Jamming movement	Low	Encoder to find error, system stops and user to contact developer.
		Loose nuts and connectors	High	Consider using reverse-thread bolts.
	MCU - Arduino	Deadlock while running	Extreme	Watchdog to reset system, safe end-stop to be assembled at movement limit.
		Faulty data caused by insufficient power supply	Medium	Internal battery pack to be equipped with voltage monitor and indicator. Safely threshold level before powering down system and inform user to charge.
	Wiring	Wiring torn or broken, hazard of electric shock	High	Safety switch at power supply to monitor system power consumption and cut supply when there is abnormality.
	Connector	Loose connector	High	Shoulder band should be implemented to position the prosthesis.
Broken joint		High	Encoder to acknowledge faulty in movement and inform watchdog to power down the system and inform user	

Table 13: Updated risk management

8. Conclusion

In conclusion, the project is timely managed, the objectives are met, and the cost analysis shows feasibility and scalability of the proposed system. The final transhumeral prosthesis is a 10 DOF mechanical arm that could perform complex movements and maintain high level of dexterity while being limited with control inputs. This design is to support amputee and congenital limb deficiency patients, whose muscles are abnormal and incapable of generating required inputs for EMG. The project takes post-assembly upgrade and maintenance into consideration to bring about a complete support system, with numerous control schemes offered by the design, cloud server for performance and model update, and user application to personalize hand grip patterns.

The project has several limitations. One of which is the use of non-invasive electrode that hinders better EEG and EMG signal acquisition. The BCI currently only supports SSVEP and alpha trigger, which also needs further research to implement motor imagery and left-right coordination.

Future work includes coming back to Vietnam for system field trial with a congenital limb deficiency patient that has previously been tested with EMG and shown positive results, working on motor imagery for BCI and designing a smaller headwear for mobility and ease of installation.

9. Reference

- [1] I. D. Federation, "IDF Diabetes Atlas," 8th ed. Brussels, Belgium, 2017.
- [2] C. McDonald, "Global incidence of major, non-datal amputation due to traumatic causes," Master, University of Washington, 2017.
- [3] S. Bhutani, J. Bhutani, A. Chhabra, and R. Uppal, "Living with Amputation: Anxiety and Depression Correlates," *Journal of Clinical and Diagnostic Research : JCDR*, vol. 10, pp. RC09-RC12, 09/01 2016.
- [4] T. C. B. Dr. Grant McGimpsey, "Limb Prosthetics Services and Devices, Critical Unmet Need: Market Analysis," B. I. C. f. Neuroprosthetics, Ed., ed: National Institute of Standards and Technology, 2017.
- [5] E. Sobotnicka and A. Sobotnicki, "BCI interface — New opportunities and hopes for the disabled. An overview of available solutions," in *2018 Baltic URSI Symposium (URSI)*, 2018, pp. 91-94.
- [6] D. J. Sturman, "Whole-hand Input," Doctor of Philosophy, School of Architecture and Planning, Massachusetts Institute of Technology, 1992.
- [7] G. Elkoura and K. Singh, "Handrix: Animating the Human Hand," presented at the Eurographics/SIGGRAPH Symposium on Computer Animation (2003).
- [8] R. J. Zenie. *Prosthetic Options for Persons with Upper-Extremity Amputation*. Available: <https://musculoskeletalkey.com/prosthetic-options-for-persons-with-upper-extremity-amputation/>
- [9] *Arm Muscle Anatomy*. Available: <https://i.pinimg.com/736x/b2/e7/83/b2e783b6e84b634e0f86b2dccb08f7d--arm-muscle-anatomy-arm-anatomy.jpg>
- [10] S. Plagenhoef, F. G. Evans, and T. Abdelnour, "Anatomical Data for Analyzing Human Motion," *Research Quarterly for Exercise and Sport*, vol. 54, pp. 169-178, 1983/06/01 1983.
- [11] S. C. Walpole, D. Prieto-Merino, P. Edwards, J. Cleland, G. Stevens, and I. Roberts, "The weight of nations: an estimation of adult human biomass," *BMC Public Health*, vol. 12, p. 439, 2012/06/18 2012.
- [12] N. I. o. Health. Body mass index table [Online]. Available: https://www.nhlbi.nih.gov/health/educational/lose_wt/BMI/bmi_tbl.pdf
- [13] R. P. N. Rao, *Brain-Computer Interfacing, An Introduction*. United States of America: Cambridge University Press, 2013.
- [14] X. M. Cohen, *Analyzing Neural Time Series Data, Theory and Practice*. London, England: The MIT Press, 2014.
- [15] N. H. Lee E. Miller, "Neuronal Activity In Motor Cortex And Related Areas," in *Brain-Computer Interfaces, Principles and Practice*, ed: Oxford University Press, Inc, 2012.
- [16] *Brain-Computer Interfaces, Principles and Practice*: Oxford University Press, Inc., 2012.
- [17] T. C. T. ldt. 10/20 System Positioning Manual [Online]. Available: https://www.transcranial.com/local/manuals/10_20_pos_man_v1_0_pdf.pdf
- [18] *International 10 - 20 System*. Available: <http://www.bem.fi/book/13/13x/1302x.htm>
- [19] W. K. Tam, K. y. Tong, F. Meng, and S. Gao, "A Minimal Set of Electrodes for Motor Imagery BCI to Control an Assistive Device in Chronic Stroke Subjects: A Multi-Session Study," *IEEE Transactions on Neural Systems and Rehabilitation Engineering*, vol. 19, pp. 617-627, 2011.
- [20] R. Prueckl and C. Guger, "A Brain-Computer Interface Based on Steady State Visual Evoked Potentials for Controlling a Robot," in *Bio-Inspired Systems: Computational and Ambient Intelligence*, Berlin, Heidelberg, 2009, pp. 690-697.
- [21] J. Zhang, C. Yan, and X. Gong, "Deep convolutional neural network for decoding motor imagery based brain computer interface," in *2017 IEEE International Conference on Signal Processing, Communications and Computing (ICSPCC)*, 2017, pp. 1-5.
- [22] T. Yu, J. Xiao, F. Wang, R. Zhang, Z. Gu, A. Cichocki, *et al.*, "Enhanced Motor Imagery Training Using a Hybrid BCI With Feedback," *IEEE Transactions on Biomedical Engineering*, vol. 62, pp. 1706-1717, 2015.
- [23] L.-W. Ko, S. S. K. Ranga, O. Komarov, and C.-C. Chen, "Development of Single-Channel Hybrid BCI System Using Motor Imagery and SSVEP," *Journal of Healthcare Engineering*, vol. 2017, p. 7, 2017.
- [24] A. Itai and A. Funase, "Simple SSVEP detection using spectrum intensity ratio and threshold," in *2013 International Symposium on Intelligent Signal Processing and Communication Systems*, 2013, pp. 722-725.
- [25] *Open Source Brain-Computer Interfaces*. Available: <https://openbci.com/>
- [26] *OpenEEG*. Available: <http://openeeg.sourceforge.net/doc/>
- [27] A. C. MettingVanRijn, A. Peper, and C. A. Grimbergen. Instrumentation Amplifiers for bioelectric events: a design with a minimal number of parts [Online]. Available: <https://www.biosemi.com/publications/artikel7.htm>
- [28] C. Moyes and M. Jiang. Brain-Computer Interface [Online]. Available: https://people.ece.cornell.edu/land/courses/ece4760/FinalProjects/s2012/cwm55/cwm55_mj294/
- [29] O. Dehzangi, Y. Zou, and R. Jafari, "Simultaneous classification of motor imagery and SSVEP EEG signals," in *2013 6th International IEEE/EMBS Conference on Neural Engineering (NER)*, 2013, pp. 1303-1306.
- [30] T. F. Bastos, S. M. T. Muller, A. B. Benevides, and M. Sarcinelli-Filho, "Robotic wheelchair commanded by SSVEP, motor imagery and word generation," in *2011 Annual International Conference of the IEEE Engineering in Medicine and Biology Society*, 2011, pp. 4753-4756.

- [31] K. Müller, "Towards robust machine learning methods for the analysis of brain data," in *2018 6th International Conference on Brain-Computer Interface (BCI)*, 2018, pp. 1-2.
- [32] E. Ventouras, M. Moatsos, C. Papageorgiou, A. Rabavilas, and N. Uzunoglu, "Independent component analysis applied to the P600 component of event-related potentials," in *The 26th Annual International Conference of the IEEE Engineering in Medicine and Biology Society*, 2004, pp. 80-83.
- [33] H. Jiang, J. P. Wachs, and B. S. Duerstock, "Integrated vision-based robotic arm interface for operators with upper limb mobility impairments," in *2013 IEEE 13th International Conference on Rehabilitation Robotics (ICORR)*, 2013, pp. 1-6.
- [34] T.-Y. Lin, M. Maire, S. Belongie, L. Bourdev, R. Girshick, J. Hays, *et al.*, "Microsoft COCO: Common Objects in Context," 2015.
- [35] PASCAL VOC project [Online]. Available: <http://host.robots.ox.ac.uk/pascal/VOC/>
- [36] J. Huang, V. Rathod, C. Sun, M. Zhu, A. Korattikara, A. Fathi, *et al.*, "Speed/accuracy trade-offs for modern convolutional object detectors," presented at the CVPR 2017, 2017.
- [37] K. Plakas and E. Trucco, "Developing a real-time, robust, video tracker," in *OCEANS 2000 MTS/IEEE Conference and Exhibition. Conference Proceedings (Cat. No.00CH37158)*, 2000, pp. 1345-1352 vol.2.
- [38] M. Ruzicka and P. Masek, "Real time visual marker detector and tracker based on computer vision for semi-autonomous convoy purpose," in *2016 17th International Conference on Mechatronics - Mechatronika (ME)*, 2016, pp. 1-6.
- [39] K. Jo, J. Im, J. Kim, and D. Kim, "A real-time multi-class multi-object tracker using YOLOv2," in *2017 IEEE International Conference on Signal and Image Processing Applications (ICSIPA)*, 2017, pp. 507-511.
- [40] W. Xin, J. v. d. Weem, and P. Jonker, "An advanced active vision system imitating human eye movements," in *2013 16th International Conference on Advanced Robotics (ICAR)*, 2013, pp. 1-6.
- [41] R. A. A. Masilang, M. K. Cabatuan, and E. P. Dadios, "Hand initialization and tracking using a modified KLT tracker for a computer vision-based breast self-examination system," in *2014 International Conference on Humanoid, Nanotechnology, Information Technology, Communication and Control, Environment and Management (HNICEM)*, 2014, pp. 1-5.
- [42] Z. Kalal, K. Mikolajczyk, and J. Matas, "Forward-Backward Error: Automatic Detection of Tracking Failures," in *2010 20th International Conference on Pattern Recognition*, 2010, pp. 2756-2759.
- [43] S. M. Davachi and B. Kaffashi, "Polylactic Acid in Medicine," *Polymer-Plastics Technology and Engineering*, vol. 54, pp. 944-967, 2015/06/23 2015.
- [44] B. Phillips, G. Zingalis, S. Ritter, and K. Mehta, "A review of current upper-limb prostheses for resource constrained settings," in *2015 IEEE Global Humanitarian Technology Conference (GHTC)*, 2015, pp. 52-58.
- [45] D. v. d. Riet, R. Stopforth, G. Bright, and O. Diegel, "An overview and comparison of upper limb prosthetics," in *2013 Africon*, 2013, pp. 1-8.
- [46] C. Toledo, L. Leija, R. Munoz, A. Vera, and A. Ramirez, "Upper limb prostheses for amputations above elbow: A review," in *2009 Pan American Health Care Exchanges*, 2009, pp. 104-108.
- [47] F. Cordella, A. L. Ciancio, R. Sacchetti, A. Davalli, A. G. Cutti, E. Guglielmelli, *et al.*, "Literature Review on Needs of Upper Limb Prosthesis Users," *Frontiers in neuroscience*, vol. 10, pp. 209-209, 2016.
- [48] S. A. Dalley, T. E. Wiste, H. A. Varol, and M. Goldfarb, "A multigrasp hand prosthesis for transradial amputees," in *2010 Annual International Conference of the IEEE Engineering in Medicine and Biology*, 2010, pp. 5062-5065.
- [49] M. Joseph T. Belter, BS, J. L. Segil, P. Aaron M. Dollar, SM, BS, and P. Richard F. Weir, "Mechanical design and performance specifications of anthropomorphic prosthetic hands: A review," *Journal of Rehabilitation Research & Development (JRRD)*, vol. 50, 2013.
- [50] G. James, *Advanced Modern Engineering Mathematics*: Prentice Hall, 2011.
- [51] D. Shira. (2018). *Vietnam: Minimum Wages on the Rise in 2018*. Available: <http://www.vietnam-briefing.com/news/vietnam-minimum-wages-on-the-rise-in-2018.html/>

10. Appendix

10.1. EEG DAQ analog board schematic

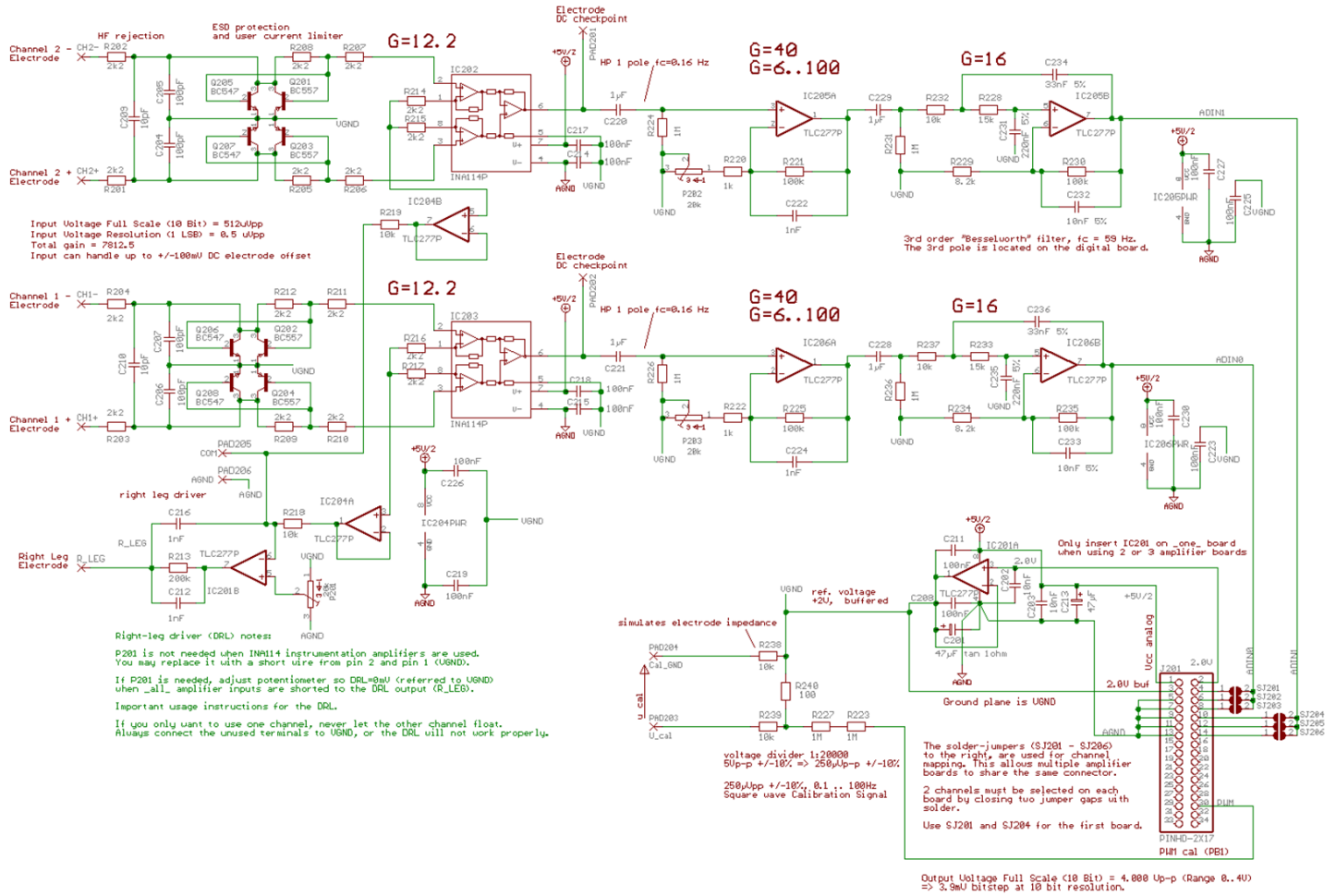


Figure 56: EEG analog board schematic

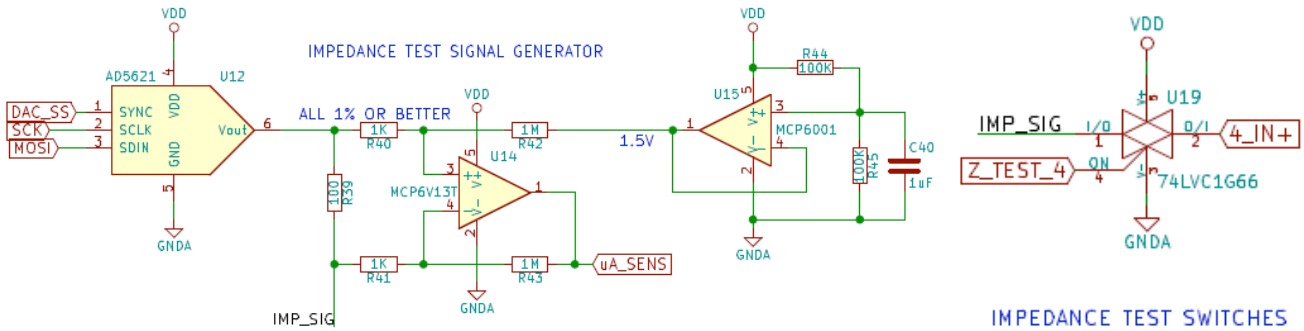


Figure 57: Impedance tester sample circuit

10.2. EEG DAQ digital board schematic

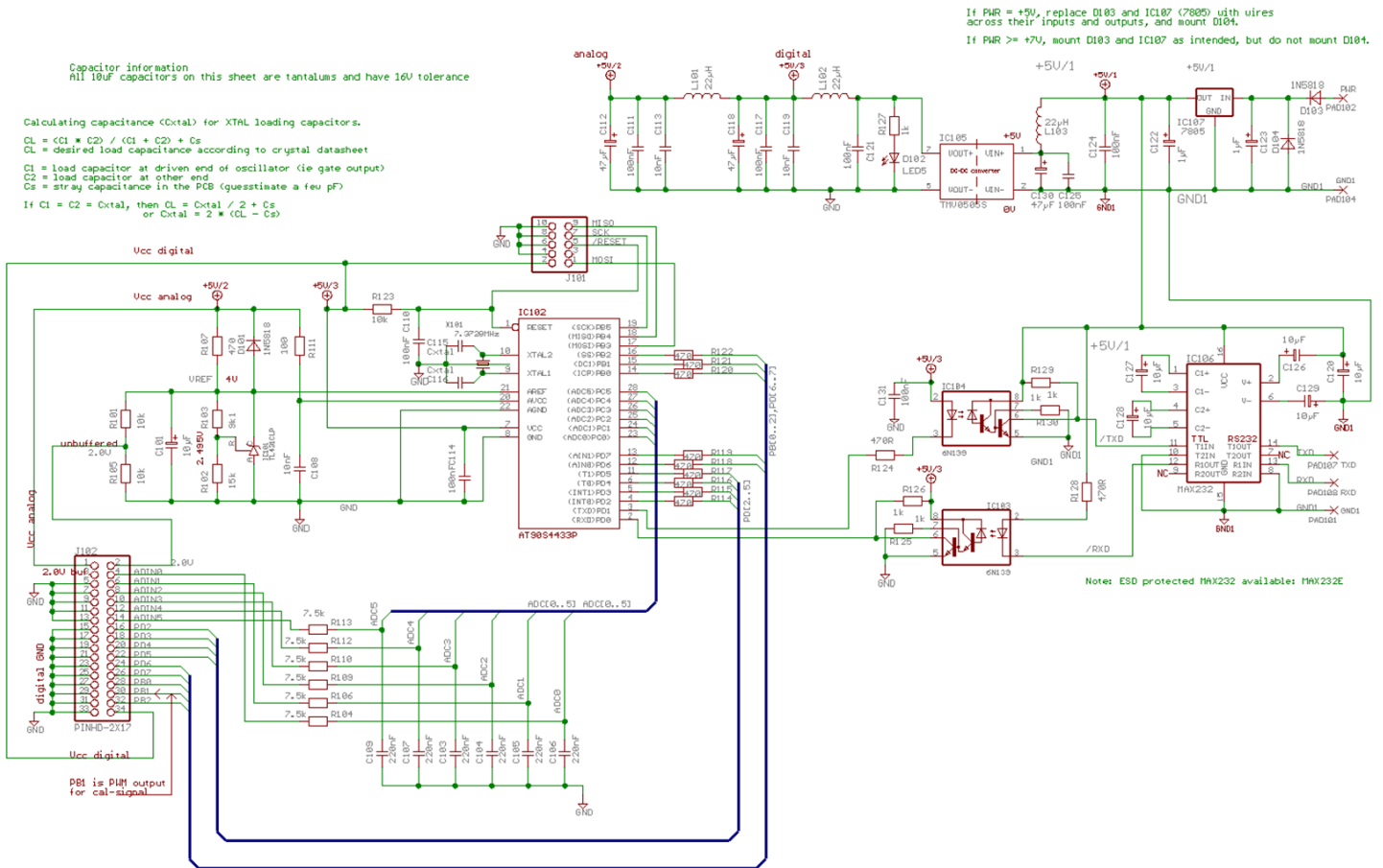


Figure 58: EEG digital board schematic